

1 **Bedrock depth influences spatial patterns of summer baseflow, temperature, and flow**  
2 **disconnection for mountainous headwater streams**

3

4

5 Martin A. Briggs<sup>1\*</sup>

6 Phillip Goodling<sup>2</sup>

7 Zachary C. Johnson<sup>3</sup>

8 Karli M. Rogers<sup>4</sup>

9 Nathaniel P. Hitt<sup>4</sup>

10 Jennifer B. Fair<sup>4,5</sup>

11 Craig D. Snyder<sup>4</sup>

12

13 <sup>1</sup>U.S. Geological Survey, Earth System Processes Division, Hydrogeophysics Branch, 11  
14 Sherman Place, Unit 5015, Storrs, CT 06269 USA

15 <sup>2</sup>U.S. Geological Survey, Maryland-Delaware-District of Columbia Water Science Center, 5522  
16 Research Park Drive, Catonsville, MD, 21228, USA

17 <sup>3</sup>U.S. Geological Survey, Washington Water Science Center, 934 Broadway, Suite 300, Tacoma,  
18 WA 98402 USA

19 <sup>4</sup>U.S. Geological Survey, Eastern Ecological Science Center, 11649 Leetown Road,  
20 Kearneysville, WV 25430 USA

21 <sup>5</sup>U.S. Geological Survey, New England Water Science Center, 10 Bearfoot Road, Northborough,  
22 MA 01532 USA

23

24 Corresponding author: Martin Briggs, [mbriggs@usgs.gov](mailto:mbriggs@usgs.gov)

25

26 **Abstract**

27 In mountain headwater streams the quality and resilience of cold-water habitat is regulated by  
28 surface stream-~~channel~~flow connectivity and groundwater exchange. These critical hydrologic  
29 processes are thought to be influenced by the stream corridor bedrock contact depth (sediment  
30 thickness), which is often inferred from sparse hillslope borehole information, piezometer  
31 refusal, and remotely sensed data. To investigate how local bedrock depth might control summer  
32 stream temperature and channel disconnection (dewatering) patterns, we measured stream  
33 corridor bedrock depth by collecting and interpreting 191 passive seismic datasets along eight  
34 headwater streams in Shenandoah National Park (Virginia USA). In addition, we used multi-year  
35 stream temperature and streamflow records to calculate summer baseflow metrics along and  
36 among the study streams. Finally, comprehensive visual surveys of stream channel dewatering  
37 were conducted in 2016, 2019, and 2021 during summer baseflow conditions (124 total km of  
38 stream length). We found that measured bedrock depths were not well-characterized by soils  
39 maps or an existing global-scale geologic dataset, where the latter overpredicted measured  
40 depths by 12.2 m (mean), or approximately four times the average bedrock depth of 2.9 m. Half  
41 of the eight study stream corridors had an average bedrock depth of less than 2 m. Of the eight  
42 study streams, Staunton River had the deepest average bedrock depth (3.4 m), the coldest  
43 summer temperature profiles, and substantially higher summer baseflow indices compared to the  
44 other study streams. Staunton River also exhibited paired air and water annual temperature signals  
45 suggesting deeper groundwater influence, and the stream channel did not dewater in lower  
46 sections during any baseflow survey. In contrast, ~~streams~~ Paine Run and Piney River did show  
47 pronounced, patchy channel dewatering, with Paine Run having dozens of discrete dry channel  
48 sections ranging 1 to greater than 300 m in length. Stream dewatering patterns were apparently

49 influenced by a combination of discrete deep bedrock (20± m±) features and more subtle  
50 sediment thickness variation (1-4 m), depending on local stream valley hydrogeology. In  
51 combination these unique datasets show the first large-scale empirical support for existing  
52 conceptual models of headwater stream disconnection based on underflow capacity and shallow  
53 groundwater supply.

54

55 **1. Introduction**

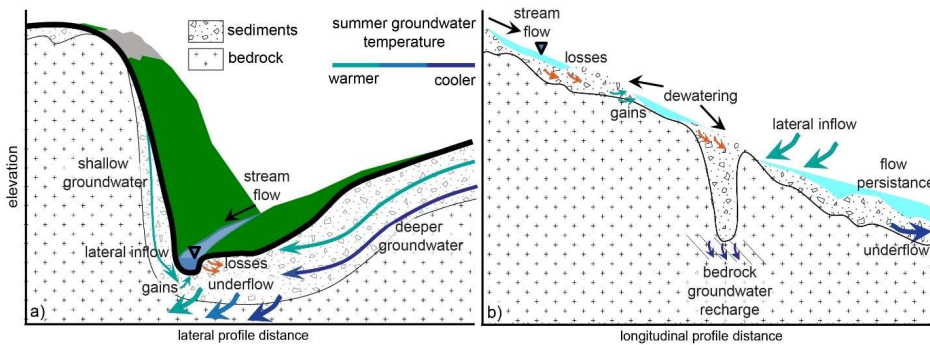
56 Mountain headwater stream habitat is influenced by hydrologic connectivity along the  
57 surface channel, and connectivity between the channel and multiscale groundwater flowpaths  
58 (Covino, 2017; Fausch et al., 2002; Wohl, 2017). Discharge from shallow groundwater within  
59 the critical zone is a primary component of stream baseflow, attenuating maximum summer  
60 temperatures and creating cold water habitat (Singha and Navarre-Sitchler, 2021; Sullivan et al.,  
61 2021) and shaping catchment topography (Litwin et al., 2022). In headwater stream valleys  
62 characterized by irregular bedrock topography and thin, permeable sediments, nested physical  
63 processes interact to control the connectivity of groundwater/surface water exchange (Tonina  
64 and Buffington, 2009). Between stormflow and snowmelt events, headwater streamflow  
65 (baseflow) is primarily generated by groundwater discharge due to a relative lack of soil water  
66 storage and release (Winter et al., 1998). Unlike in lower valley settings, mountain headwaters  
67 accumulate ~~reduced-less~~ fine soil, facilitating efficient routing of quickflow to streams through  
68 macropores and other preferential flowpaths within regolith and saprolite (Sidle et al., 2000).  
69 Recharge that does percolate vertically contributes to shallow groundwater along steep hillslopes  
70 and valley floors, where groundwater flowpath depths are constrained by bedrock topography  
71 (Buttle et al., 2004). Although deeper groundwater may also represent an important contribution  
72 to summer streamflow in systems with relatively permeable bedrock (Burns et al., 1998;  
73 O’Sullivan et al., 2020), shallow, low permeability bedrock generally restricts stream-  
74 groundwater connectivity to the thin layers of unconsolidated sediments (Briggs et al., 2018b).

75 In addition to baseflow drainage along headwater stream networks, down-valley shallow  
76 groundwater ‘underflow’ can be substantial when high gradient streams lack sinuosity and flow  
77 over permeable sediment (Figure 1a, Figure A1). In fact, headwater stream channels may only be  
78 expected to show surface flow when the transmission ability of the underlying alluvium and

79 colluvium is exceeded, and bedrock depth is thought [to be](#) a primary control of this underflow  
80 capacity (Ward et al., 2020). In some hydrogeologic settings, underflow can dominate  
81 groundwater export from mountain catchments compared to groundwater drainage via the  
82 surficial stream channel (Larkin and Sharp, 1992; Tiwari et al., 2017). Moreover, in addition to  
83 longitudinal transport down-valley, underflow also acts as a reservoir of exchange for hyporheic  
84 flowpaths that may mix with shallow groundwater before returning to channel flow (Payn et al.,  
85 2009), transporting buffered temperature signals back to channel waters (Wu et al., 2020). Local  
86 underflow is recharged from upgradient flowpaths and adjacent hillslopes, creating complex  
87 seasonal and interannual patterns in groundwater connectivity and discharge to surface water  
88 (Jencso et al., 2010; Johnson et al., 2017). A major challenge to understanding groundwater  
89 exchange in headwaters is that attributes of the streambed subsurface, such as the depth to the  
90 underlying bedrock contact, are often only available from limited direct measurements, coarse  
91 spatial interpolations, or inferred remotely based on landscape forms. Therefore, methods that  
92 allow efficient, local measurements of the streambed subsurface are critically needed.

93         Seasonal thermal regimes of mountain headwater streams can be profoundly impacted by  
94 groundwater inflow from multiple depths (Briggs et al 2018a). In lower valley settings, the  
95 temperature of groundwater discharge along stream networks is often assumed to [be constant](#)  
96 [throughout the year and](#) approximate the average annual land surface temperature ~~throughout the~~  
97 ~~year~~ (Stonestrom and Constantz, 2003). Conversely, shallow groundwater temperature (within  
98 several m from land surface) can show pronounced seasonality (Bundschuh, 1993; Lapham,  
99 1989) and high spatial variability, even over small spatial extents (Snyder et al. 2015). The  
100 warming of shallow groundwater during the summer and fall seasons can limit the ability of  
101 gaining mountain streams to support cold-water fish populations during the low flow season,

102 even if baseflow (assumed to be dominated by groundwater discharge) fractions are large  
 103 (Johnson et al., 2020). In systems with low permeability bedrock, thicker hillslope sediments  
 104 may generate deeper, colder lateral groundwater flow to streams in summer (Figure 1a),  
 105 increasing cold water habitat resiliency (Briggs et al., 2018b). For example, a recent meta-  
 106 analysis of stream and air temperature records across the contiguous United States found that a  
 107 substantial fraction of shallow groundwater dominated streams displayed summer warming  
 108 trends in recent decades, while deeper groundwater dominated streams were more stable (Hare et  
 109 al., 2021). Steep mountain stream systems such as those found in the Blue Ridge and Cascade  
 110 mountains of the USA have been found to show annual thermal regimes dominated by the annual  
 111 thermal signals indicative of shallow groundwater (Johnson et al., 2020), indicating such streams  
 112 may also be at risk for warming over time, contrary to assumptions based on elevation alone.



113  
 114 *Figure 1. A conceptual mountain stream valley cross section (panel a) and longitudinal profile*  
 115 *(panel b) indicating the expected control of low permeability bedrock topography on*  
 116 *groundwater temperature, stream-groundwater exchange, patchy stream dewatering, and the*  
 117 *underflow reservoir.*

118 Beyond warm summer stream temperatures, the dewatering and disconnection of the  
 119 active stream channel during summer low flows can adversely impact fish habitat by impeding  
 120 fish movement (Edge et al., 2017; Labbe & Fausch, 2000; Rolls et al., 2012; Snyder et al.,  
 121 2013), locally degrading water quality (Hopper et al., 2020), and increasing predation risks in

122 isolated pools (Magoulick and Kobza 2003). However, the physical controls on localized stream  
123 channel dewatering are not well characterized and likely involve a spectrum of nested gaining  
124 and losing flowpaths. For mountain headwater streams, previous research has documented major  
125 contractions of drainage networks during seasonal drydown (Ilja Van Meerveld et al., 2019) and  
126 general seasonal shifts in hydraulic gradients from gaining to losing, with closely coupled  
127 streamflow and precipitation events, indicating a dominance of shallow routing rather than  
128 deeper groundwater connectivity in maintaining streamflow (Zimmer and McGlynn, 2017).  
129 ~~Warix et al., (2021) found that although deeper/older groundwater was found to contribute to~~  
130 ~~their study streams during dry down, those sources were insufficient in preventing dry channel~~  
131 ~~sections from occurring, also indicating the importance of shallow groundwater inflows and local~~  
132 ~~geologic controls.~~ Locally-losing sections of headwater stream channels can be associated with  
133 coarse, permeable colluvial deposits from hillslope mass wasting processes (Costigan et al.,  
134 2016; Weekes et al., 2015), as local enhancement of the total pore space under mountain streams  
135 can drive downwelling of streamwater (Figure 1b, Tonina & Buffington, 2009). Main channel  
136 dewatering occurs when the bed sediments have a storage and transport capacity that exceeds  
137 stream discharge (Rolls et al., 2012; Ward et al., 2018), though stream water losses can also be  
138 driven by local changes in bed morphology and slope (Costigan et al., 2016) and bedrock  
139 permeability. The shallowing of the underlying bedrock contact may drive lateral underflow  
140 toward the surface causing the channel to gain water (Herzog et al., 2019, ~~Figure 1b~~), though  
141 such hypothesized dynamics are not well documented in existing literature due to a relative lack  
142 of bedrock topography data along headwater streams.

143 At large scales, contiguous bedrock depth layers are interpolated from a combination of  
144 relatively sparse borehole data and surface topography (Kauffman et al., 2018; Pelletier et al.,

Field Code Changed

145 2016; Shangguan et al., 2017). However, in steep headwater systems with little borehole data,  
146 bedrock topography is difficult to predict accurately from land surface topography alone. The  
147 development of improved tools for predicting bedrock depth is an active area of research which  
148 has recently demonstrated promise when bedrock outcrop data are included (e.g. Furze et al.,  
149 2021; Odom et al., 2021). The limitations of using landform data to predict bedrock depth are  
150 compounded by inherent challenges in collecting physical data via soil pits and monitoring wells  
151 in rugged, rocky terrain, and so direct measurement data are often limited to highly studied  
152 experimental watersheds where bedrock depth is *still only inferred* from piezometer installation  
153 refusal (e.g. Jencso et al., 2010; Ward et al., 2018). In more typical headwater systems, existing  
154 wells may be preferentially installed to maximize the production of water and not broadly sample  
155 the true range of bedrock depths.

Formatted: Font: Italic

156 Application of near surface geophysical methods to stream corridor research has  
157 increased appreciably in recent years (McLachlan et al., 2017), and several methods are sensitive  
158 to shallow subsurface flow and geologic attributes including bedrock depth. Active seismic  
159 refraction measurements can provide high resolution (10s of cm) bedrock depth information  
160 along transect-based cross-sections (e.g. Flinchum et al., 2018), but are less suited for  
161 exploration throughout rugged mountain stream valleys at the many km-scale due to logistical  
162 challenges in using active seismic methods to obtain a sufficient amount of data to effectively  
163 characterize important variation in bedrock depth at relatively small, ecologically-relevant spatial  
164 scales.

165 Point-based, efficient passive seismic measurements represent a unique combination of  
166 high mobility and relative precision for measuring bedrock depth along mountain valleys. The  
167 horizontal-to-vertical spectral ratio (HVSr) method is a passive seismic technique that evaluates

168 ambient seismic noise recorded using handheld instruments placed on the ground surface to  
169 identify seismic resonance that develops due to strong vertical changes in subsurface acoustic  
170 impedance, which occurs at distinct unconsolidated sediment/bedrock interfaces (Yanamaka et  
171 al., 1994). While typically insensitive to variations in unconsolidated sediment permeability (i.e.,  
172 clay lenses), the HVSR method is effective at identifying the depth to distinct unconsolidated  
173 sediment/bedrock interfaces at essentially the ‘point’ spatial scale, HVSR measurements are  
174 often not successful in settings with highly weathered bedrock surfaces such as those with  
175 pronounced epikarst and saprolite.

176 The control of stream to groundwater exchange (i.e., ‘transmission losses’) on streamflow  
177 permanence has been highlighted as an important research need by the comprehensive review  
178 of intermittent stream systems by Costigan et al., (2016). Following the conceptual model of  
179 Ward et al., (2018) for mountain stream corridors, a central hypothesis of our research was that  
180 bedrock depth along the stream corridor will act as a first-order control on stream dewatering  
181 patterns when shallow bedrock is of low permeability. Based on the concepts presented by  
182 Tonina & Buffington, (2009), we postulated that relatively thick, permeable surficial sediment  
183 zones could locally accommodate the entirety of low streamflow volumes, dewatering main  
184 channel sections at varied scales when not balanced by groundwater inflow (Figure 1b). We  
185 further hypothesized that summer stream channel thermal regimes would also be influenced by  
186 bedrock depth, as the temperature of groundwater flowpaths that generate baseflow is depth  
187 dependent (Briggs et al., 2018b), indicated conceptually in Figure 1a. To test our hypotheses, we  
188 extended the existing mountain headwater bedrock depth surveys from Shenandoah National  
189 Park (SNP), Virginia, USA (citation) to seven additional subwatersheds and compared results to  
190 physical mapping of stream dewatering, multi-year stream temperature data and derived

Formatted: Font: (Default) Times New Roman

Formatted: Font: (Default) Times New Roman

Formatted: Font: (Default) Times New Roman

191 groundwater influence metrics, and baseflow separation analysis to address the following  
192 research questions:

- 193 1. Does stream corridor bedrock depth exhibit longitudinal spatial structure in mountainous  
194 streams [at ecologically relevant spatial scales](#)? Can measured bedrock depth dynamics be  
195 accurately extracted from existing large-scale datasets or inferred from high resolution soils  
196 maps?
- 197 2. Does underflow generally represent a net source or sink of summer flow for headwater  
198 streams based on observed dewatering patterns and groundwater influence metrics?
- 199 3. Does bedrock depth explain spatial variation in stream temperature and summer baseflow  
200 indices within headwater streams?

## 201 **2. Study Area**

202 The SNP is an 800 km<sup>2</sup> area of preserved headwater forest perched along a major  
203 ridgeline of the Blue Ridge Mountains in northern VA, USA (Figure 2). The bedrock of the park  
204 is predominantly low permeability basaltic and granitic material in the central and northern  
205 sections, and siliciclastic along the southern section (Southworth et al., 2009), though many  
206 subwatersheds also transition in dominant bedrock type [from high to lower elevation](#). Stream  
207 valleys of SNP are typically steep and feature a perennial channel with mainly non-perennial  
208 tributaries (Johnson et al., 2017), Figure A1) and stream baseflow consists of less than 3-yr old  
209 groundwater on average (Plummer et al., 2001). In contrast, water collected from SNP hillslope  
210 wells completed in shallow fractured rock generally have higher ages of 10-20 yr (Plummer et  
211 al., 2001), indicating minimal contributions from bedrock groundwater to streamflow. Previous  
212 ecohydrological research in SNP has noted that some mainstem stream channels show patchy

213 dewatering at summer low flows (Snyder et al., 2013), though the physical controls on these  
214 patterns of stream drying were not clear.

215 In SNP, stream baseflow is thought to be predominantly generated by near-surface  
216 drainage of coarse unconsolidated alluvium and colluvium (DeKay, 1972; Nelms and Moberg,  
217 2010). The mountain ridgeline streamflow systems are expected to drain near-surface flowpaths  
218 and accommodate substantial down valley underflow below perennial stream channels (Figure  
219 A1). A portion of hillslope recharge is expected to percolate downward through connected  
220 bedrock fractures into the deeper groundwater reservoir contributing to mountain block recharge  
221 along the Shenandoah River Valley. Narrow alluvium deposits mapped along the stream  
222 corridors of SNP are thought to generally range up to 6 m in thickness and be more clay rich  
223 when sourced by basaltic bedrock (Southworth et al., 2009). Data at sparse wells drilled along  
224 the SNP ridgeline indicate bedrock depth can range over 20 m on hillslopes and be highly  
225 variable (DeKay, 1972; Goodling et al., 2020; Lynch, 1987).

226 Previous research has inferred summer and annual groundwater discharge patterns  
227 throughout SNP subwatersheds based on paired, local air and stream water temperature  
228 dynamics (Briggs et al., 2018a; Johnson et al., 2017; Snyder et al., 2015). Combined, these  
229 analyses indicated groundwater exchange is highly variable in space along singular stream  
230 valleys and between subwatersheds, and dependent upon local- to subwatershed-scale  
231 characteristics. A combination of landform features that include stream slope and stream valley  
232 confinement operate in conjunction with seasonal precipitation to drive groundwater influence  
233 on summer stream temperatures (Johnson et al., 2017). Multi-week lags in time between  
234 streamwater and local air annual temperature signals (i.e., [water](#) phase shifts toward later time)  
235 were observed from dozens of the 120 total monitored stream sites indicating a dominance of

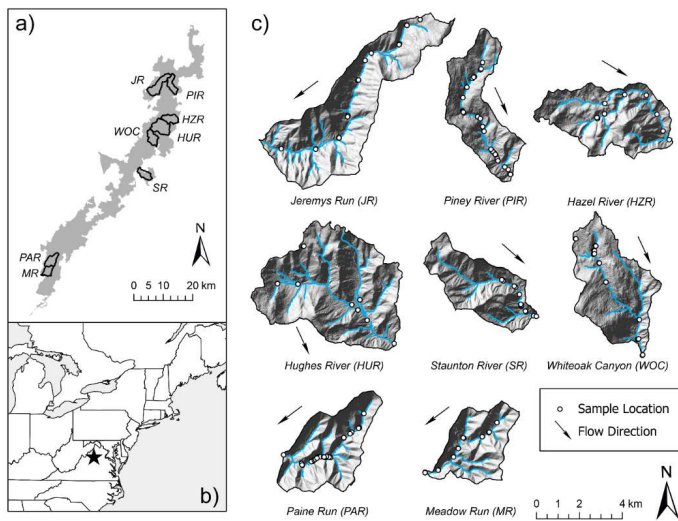
236 shallow groundwater discharge, originating generally within approximately 3 m of land surface  
237 (Briggs et al., 2018a).

238

239

240

241



242

243 *Figure 2. This study was based in Shenandoah National Park (panel a) located in the Blue Ridge*  
244 *Mountains of northeast USA (panel b). LiDAR hillshade cutouts of each subwatershed illustrate*  
245 *the rugged terrain and varied valley morphology (panel c). The mainstem stream channel and*  
246 *tributaries are traced and HVSR-passive seismic sample measurement locations noted.*

### 247 3.0 Methods

#### 248 3.1 Passive Seismic Bedrock Depth Measurements

249 Periodically from the summer of 2016 to the spring of 2020, we acquired 323 HVSR  
250 measurements across SNP. The geophysical data were collected along the perennial streams of

251 seven subwatersheds with extensive existing stream temperature and ecological datasets, and at  
252 known ridgeline and hillslope borehole locations. This effort added to previously interpreted  
253 HVSR data from 22 riparian sites collected along the Whiteoak Canyon subwatershed in late  
254 2015 (Briggs et al., 2017), for a total of 8 mountain streams for analysis in this study (Figure 2).  
255 In July 2016, HVSR data were collected in the following subwatersheds: Piney River, Paine  
256 Run, Meadow Run, Jeremy'sJeremys Run, Hazel River, and Hughes River. Some stream  
257 sections were inaccessible due to steep bedrock walls and waterfalls, resulting in poor data  
258 coverage in those areas.



259 *Figure 3. Typical sections of a) Paine Run, b) Piney River, c) Staunton River, and d) a section of*  
260 *Paine Run that was dewatered at baseflow leaving isolated pools. The passive seismic HVSR*  
261 *instruments are shown deployed in panels a), b) and d) (Photographs by the U.S. Geological*  
262 *Survey).*  
263  
264

265 Measurement locations mostly coincided with existing stream temperature monitoring  
266 stations (described by Snyder et al., 2017), and were typically made at points immediately  
267 adjacent to the stream or on larger rocks within the channel (Figure 3). In July 2019, HVSR data  
268 were again collected along Paine Run and Piney River subwatersheds, and throughout the lower  
269 Staunton River (Figure 3). The 2019 survey design differed in that transect measurements were  
270 made at 4 locations along the stream channel waterline spaced approximately 25 m apart at  
271 longitudinal locations that differed from the 2016 survey. This was done to assess potential  
272 variation in bedrock depth along short subreaches of these three streams. Finally, clustered  
273 HVSR data were collected in March 2020 in Paine Run and Piney River in zones previously  
274 observed to show channel disconnection and streamflow re-emergence. Measurement locations  
275 were chosen to test the hypothesis that the dewatering patterns were controlled by bedrock depth  
276 as shown conceptually in Figure 1b.

277 HVSR data were collected using multi-component Tromino seismometers (MOHO,  
278 S.R.L.) directly coupled to the land surface or placed on heavy metal plates where sediment was  
279 loose. Collection times ranged 10-20 min at either 128 or 256 Hz sampling rates. HVSR data  
280 collection locations were determined by a combination of internal Tromino GPS and external  
281 GPS units. HVSR measurements were processed to derive a resonant frequency using a  
282 commercially available program (GRILLA® v. 8.0 (2018); further details regarding data  
283 processing are given by Goodling et al., (2020).

284 Resonant frequency measurements that passed a series of quality criteria were then  
285 converted to a bedrock depth estimate following Briggs et al., (2017). This conversion  
286 necessitates a shear wave velocity estimate for the unconsolidated sediments over bedrock.  
287 HVSR data collected at [six](#) spatially distributed boreholes with documented depth to varied-type

288 bedrock along the SNP ridgeline indicated a [mean](#) shear wave velocity of 358.7 +/- 56 m/s  
289 (Goodling et al., 2020). A similar shear wave velocity of 346 m/s was measured at two locations  
290 along the Whiteoak Canyon riparian zone spaced several km apart using active seismic methods  
291 (Briggs et al., 2018b). This agreement indicates a common shear wave velocity can be assumed  
292 for the unconsolidated material of SNP subwatersheds. For this study we used the average of  
293 these spatially distributed active and passive seismic methods at 352 m/s. The [mean-average](#)  
294 shear wave velocity calculated in this study is comparable to the mean shear wave velocity  
295 ranges in firm soils (180 - 360 m/s) and very dense soil and soft rock (360-760 m/s), according to  
296 National Earthquake Hazards Reduction Program (NEHRP) guidelines (Building Seismic Safety  
297 Council, 1994). As an example of measurement sensitivity to the shear wave velocity parameter  
298 for shallow bedrock contacts, a velocity change in either direction by 25 m/s would generally  
299 shift the bedrock depth estimate by <0.2 m.

### 300 *3.2 Observations of spatial dewatering patterns*

301 Longitudinal (upstream to downstream) patterns of dewatering were determined in the  
302 summers of 2016, 2019, and 2021 during baseflow conditions over 124 total km of stream length  
303 for all surveys combined. In July-August of 2016 all eight subwatersheds (Figure 2) were  
304 surveyed. In September of 2019 and August 2021, dewatering surveys were repeated in three  
305 subwatersheds (Paine Run, Piney River, and Staunton River) to evaluate annual variation in  
306 dewatering patterns. Data were collected by [a](#) team of investigators walking each stream from an  
307 upstream location defined by the point along the stream draining 75-hectares (assumed capture  
308 area required to generate perennial streamflow, determined using watershed tools in ArcGIS) to  
309 the bottom of each watershed near the park boundary, and mapping transition points between  
310 three hydrologic categories: Wet, dry, or isolated pools based upon investigator observation.  
311 “Wet” segments were defined as reaches where entire channel was wet with flow between pools;

312 “Dry” segments were defined as reaches containing no water, or isolated pools of insufficient  
313 depth to sustain 1+ year old brook trout; and “Isolated Pools” were defined as reaches containing  
314 pools of sufficient depth to support brook trout but were hydrologically disconnected from other  
315 parts of the channel. An example of isolated pools is photographically depicted in Figure 3d.  
316 Spatial coordinates of transition points were mapped using a Trimble R2 GNSS receiver for <1-  
317 meter accuracy. Surveys for each subwatershed were completed within a single day to minimize  
318 effects of temporal variation in precipitation.

319 In addition to local variability in bedrock depth, spatial patterns of dewatering and stream  
320 temperature are likely to be influenced by seasonal precipitation and air temperature proximate  
321 to the period of measurement (i.e., summer conditions, 2016 and 2019). We used historical  
322 weather records (1942 – 2020) collected from the nearby Luray Weather Station located within  
323 SNP (Station No. GHCND:USC00445096) to compare weather conditions during these two  
324 study years with historical norms. Finally, 3D surface area of each subwatershed was determined  
325 from existing LiDAR data using [the Add Surface Information tool in 3D Analyst Tools](#) in  
326 ArcGIS and mean valley [bottom](#) width was evaluated from LiDAR data using 100-m transects  
327 measured approximately 2 m above the valley floor.

### 328 *3.3 Stream channel temperature data and baseflow separation*

329 Multi-year SNP stream temperature data were collected at hourly time intervals as  
330 described by Snyder et al., (2017) using HOBO Pro V2 thermographs (+/- 0.2 °C expected  
331 accuracy). From this larger dataset, 64 main channel locations within the 8 study subwatersheds  
332 were extracted and processed for summary statistics such as the maximum and minimum of the  
333 7-day running mean using Matlab R2019b software (Mathworks, Inc.). Only complete 7-day  
334 periods were included in the running average. Warm season data (July, August, September) were

335 isolated and analyzed to coincide with the stream dewatering surveys and a larger body of  
336 research regarding summer cold-water brook trout habitat in SNP. We utilized stream  
337 temperature data processed to extract annual temperature signals by Briggs et al., (2018a) where  
338 dry sensor periods were identified and removed, impacting a handful of the upper stream sites.  
339 Data were visualized and downstream trends explored using Sigmaplot 14.0 software (Systat  
340 Software Inc.). Baseflow separation was conducted for the three continuously gaged streams of  
341 this study (Paine Run, Piney River, Staunton River) over summer months for the period of record  
342 (1993-2020). Following the approach of (Hare et al., (2021), the daily Baseflow Index (BFI) was  
343 calculated using the USGS-R 'DVstats' package (version 0.3.4) by following methods  
344 described by (Barlow et al., (2014), and dividing the calculated baseflow discharge by the  
345 corresponding stream discharge, where a value of one would indicate stream discharge was  
346 entirely composed of baseflow. BFI was then averaged (mean) across each summer season,  
347 along with the mean and standard deviation of summer stream discharge.

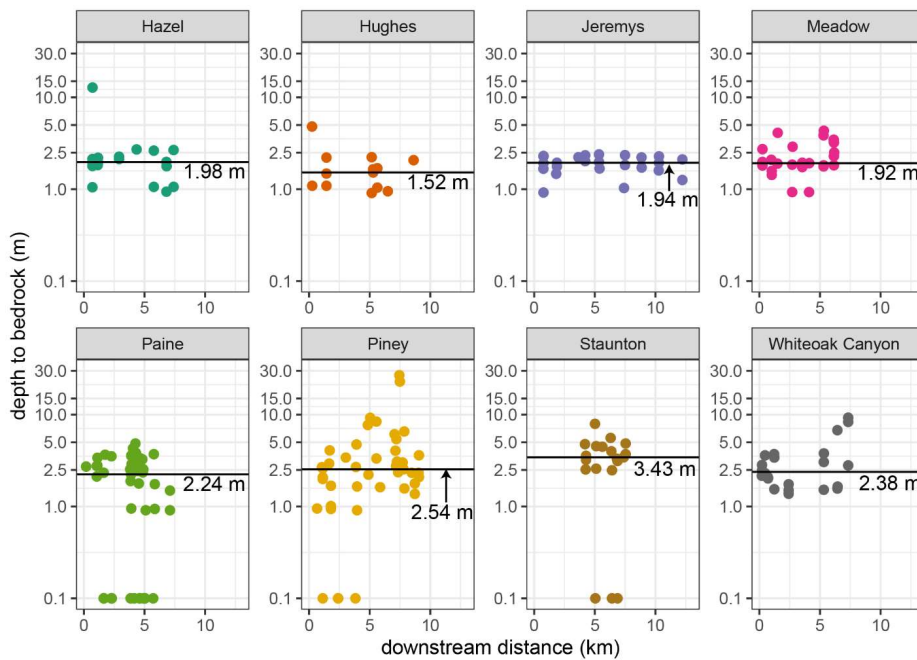
## 348 **4. Results**

### 349 *4.1 Stream Corridor Bedrock depth*

350 Approximately 60% of individual HVSR measurements (191 of the 323) were of high  
351 enough quality to be interpreted for bedrock depth using objective data quality metrics reported  
352 by the GRILLA software. This ratio of interpretable to total HVSR measurements was similar to  
353 the previous 2015 Whiteoak Canyon Run study using the same instrument type (Briggs et al.,  
354 2017). For the 132 datasets that could not be interpreted, the primary reason was no identifiably  
355 resonant frequency 'peak' in the multicomponent seismic data, as described in more detail in the  
356 data release of Goodling et al., (2020). The loosely consolidated, rocky surficial soils of many  
357 SNP subwatershed riparian zones likely contributed to poor instrument coupling to the land

358 surface, and therefore reduced measurement sensitivity/success compared to firmer soils.  
 359 However, due to spatial redundancy in the measurements, the 191 locations where bedrock depth  
 360 was evaluated generally covered all the intended longitudinal stream measurement locations  
 361 throughout the subwatersheds.

362



363

364 *Figure 4. Measured depth to rock along the stream channel and riparian zones of the eight study*  
 365 *subwatersheds. Exposed bedrock (i.e., zero depth) observed at the intended measurement*  
 366 *location is noted here by a value of '0.1' on the log scale. The median value is shown as a*  
 367 *labelled horizontal line.*

368

369 The median bedrock depth was smallest for Hughes River (1.52 m), and similar for  
 370 Meadow Run, ~~Jeremy's~~Jeremys Run, Hazel River (1.92, 1.94, 1.98, respectively, Table 1, Table  
 371 B1, Figure 4). Paine Run had a median of 2.24 m, Whiteoak Canyon of 2.38 m, and Piney River

372 of 2.54 m. Lower Staunton River had the largest median depth to rock of 3.43 m (Table 1). Piney  
 373 River had the largest variation in bedrock depth, including a discrete zone greater than 20 m  
 374 deep, along with several zones of exposed bedrock along the channel. Visual observations of  
 375 exposed channel bedrock were not incorporated into the bedrock depth averages presented in  
 376 Table 1. Simple bivariate relations were explored between the physical valley parameters, and a  
 377 negative relation was found between bedrock depth and mean valley bottom width while other  
 378 relations were not significant.

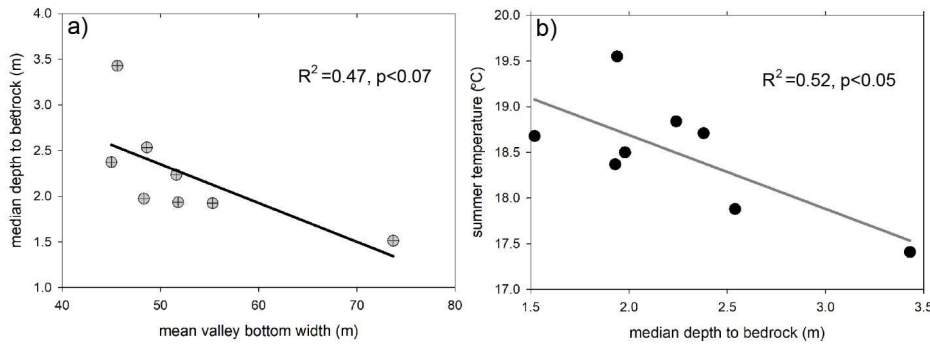
379 **Table 1.** The median bedrock depth along with the elevation, mean, and 7-d maximum summer  
 380 temperatures over the period of record collected at most downstream site location in each  
 381 subwatershed.

site	3D subwatershed surface area (km <sup>2</sup> )	mean valley bottom width (m)	median bedrock depth (m)	mean stream slope (°)	most downstream stream temperature site		
					elevation (m)	mean (°C)	7-d max (°C)
Hughes River	42.2	73.7	1.52	22.7	307	18.7	21.2
Meadow Run	15.0	55.3	1.93	14.2	450	18.4	20.4
Jeremy's Jeremys Run	37.5	51.8	1.94	16.3	286	19.6	23.6
Hazel River	22.5	48.3	1.98	13.0	328	18.5	21.7
Paine Run	21.7	51.6	2.24	15.6	426	18.8	20.9
Whiteoak Cyn.	22.4	45.0	2.38	17.2	348	18.7	21.2
Piney River	20.6	48.6	2.54	14.9	371	17.9	20.6
Staunton River	18.0	45.6	3.43	20.7	309	17.4	19.9

Formatted Table

Formatted Table

382

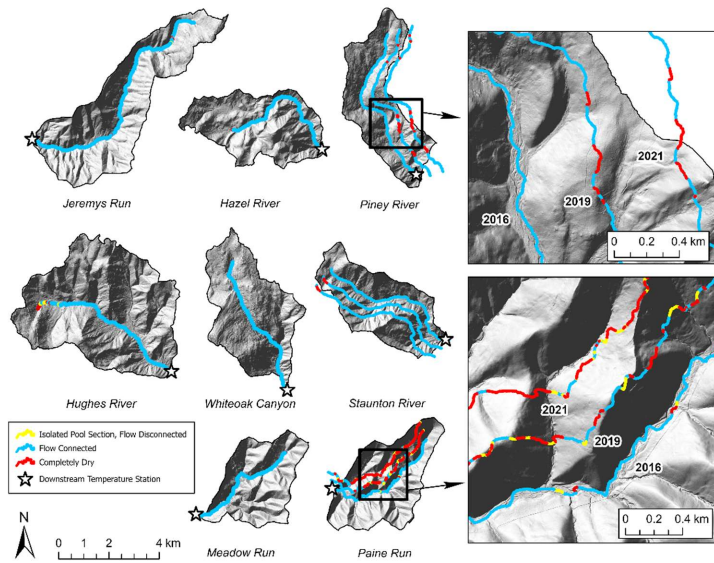


383

384 *Figure 5. Median study stream corridor bedrock depth showed a negative relation to valley*  
385 *bottom width (panel a), and mean summer stream temperature at the lower study stream*  
386 *boundaries was negatively related to median bedrock depth (panel b).*

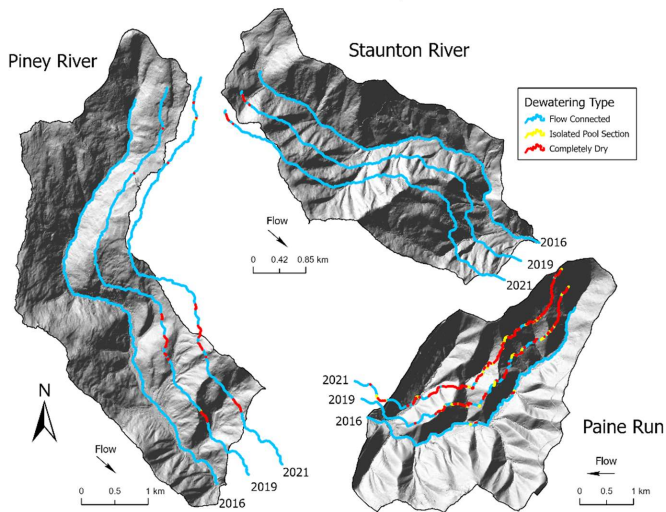
#### 388 4.2 Spatial Dewatering Patterns and Climate Data

389 Cumulative monthly precipitation during baseflow summer (July-September) was higher  
390 than normal in 2016 and near average or lower than average (period of record 1942-2020),  
391 depending on the month, in 2019 (Figure A2). Mean monthly air temperatures were higher than  
392 average for both study years during baseflow summer reflecting the long-term trend of  
393 increasing air temperatures in the park (Luray weather station GHCND:USC00445096);-see  
394 [Menne et al. 2012](#)). Patches of stream dewatering were observed along five of the eight study  
395 subwatersheds between 19-27 July, 2016, when over 98 km of total stream length were mapped  
396 (Figure 65). However, for Meadow Run, Hazel River, and Hughes River stream dewatering only  
397 occurred near the upper stream origination point. In contrast, Paine Run and ~~Jeremy's~~Jeremys  
398 Run had several discrete dewatering sections further from their origination points (examples  
399 shown in Figure 3d, Figure A3). During the drier period 17-19 September 2019, no dewatering  
400 was found along lower Staunton River, though Piney River had seven discrete dry patches where  
401 none were mapped in 2016, and similar patterns were observed for those two streams in 2021  
402 (Figure 76). Paine Run had 29 points of dewatering in 2019, distributed mainly along the central  
403 and upper sections of the stream corridor, and showed extensive dewatering in 2021 (Figures 65,  
404 76, 87). The two Paine locations that were dry in 2016 were also dry in 2019 and 2021.



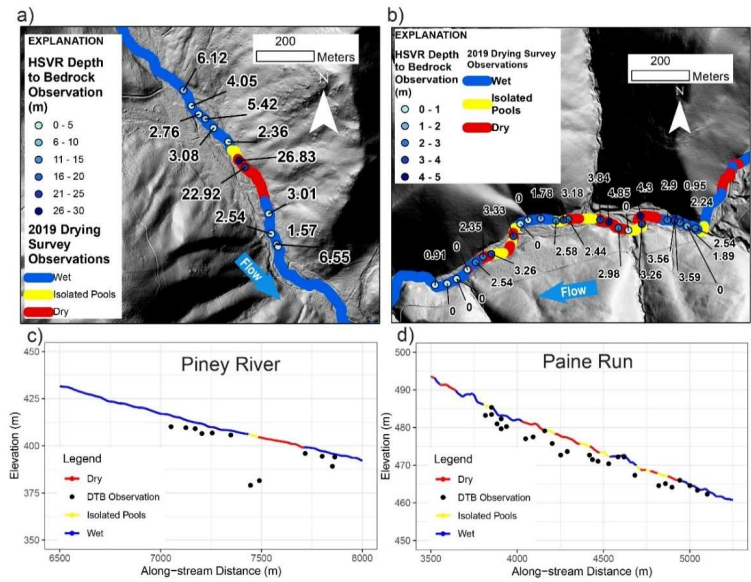
405

406 *Figure 65. Results from 2016, 2019, and 2021 longitudinal channel dewatering surveys*  
 407 *conducted by physical observation, where the 2019 and 2021 data are shown offset laterally*  
 408 *from the stream channel where those surveys occurred.*



409

410 Figure 76. Zoom views for the three study watersheds where stream dewatering observations  
 411 were also collected in 2021 over three summer seasons (2016, 2019, 2021):-  
 412  
 413  
 414

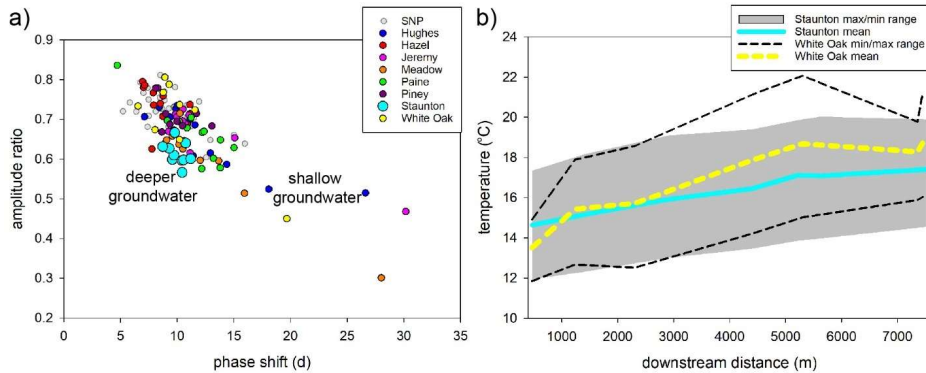


415  
 416 Figure 87. The results of the 2019 stream drying survey and 2020 high spatial resolution HVS  
 417 measurements are shown over the LiDAR hillshade in plan view (panels a, b) and along a  
 418 LiDAR-derived stream elevation profile cross-section view (panels c, d) for Piney River (panels  
 419 a, c) and Paine Run (panels b, d).

#### 420 4.3 Stream Temperature Patterns

421 Paired air and water annual temperature signals exhibited a spectrum of shallow  
 422 groundwater influences as indicated by extracting fundamental sinusoids from each multi-year  
 423 temperature dataset per methods described by Briggs et al. (2018). Observed phase shifts  
 424 between stream and local air temperature signals ranged from approximately 5 to 30 d with a  
 425 mean of 11 d. Reduced annual temperature signal amplitude ratio generally corresponded with  
 426 increased phase shift when all SNP stream monitoring sites are plotted in aggregate (Figure 98a).

427 Staunton River stream sites cluster together and show less signal phase shift (mean of 10 d) for  
428 similar<sup>ly</sup> low amplitude ratio values (mean of 0.6) observed in other subwatersheds.



429

430 *Figure 98. Panel a) shows the annual temperature signal metrics for the study subwatersheds*  
431 *highlighted within the larger SNP dataset with conceptual groundwater end member signature*  
432 *trajectories. Panel b) displays the downstream mean summer temperature profiles and 7-d*  
433 *maximum and minimum temperature ranges for Staunton River and Whiteoak Canyon.*

434

435 Although originating in a similar place (Table 1), the downstream mean, 7-d maximum,  
436 and 7-d minimum stream temperature profiles differed between Staunton River and Whiteoak

437 Canyon, where the latter had greater temperature variation and warming with downstream

438 distance (Figure 98b). The mean summer stream temperature had an approximate 2 °C total

439 range over the period of record. The warmest average (19.6 °C) and 7-d maximum (23.6 °C) was

440 observed for the lower ~~Jeremy's~~Jeremys Run site, which was also at the lowest elevation.

441 However, only 23 m higher in elevation, the downstream Staunton River site had the coldest

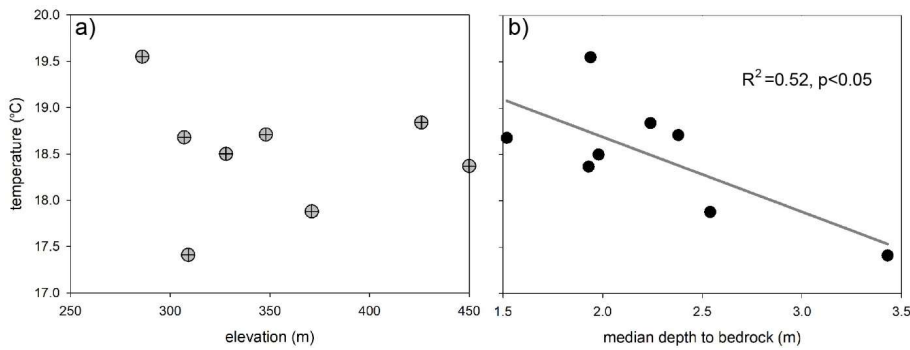
442 average (17.4 °C) and 7-d maximum (19.9 °C) summer temperature. Piney River, which has the

443 second largest median bedrock depth (2.54 m), had the second lowest average temperature (17.4

444 °C) at the lower site. No significant relation was observed between elevation and mean summer

445 temperature at the lower stream monitoring site, (Figure 9a), but a significant negative linear

446 relation ( $R^2=0.52$ ;  $p<0.05$ ) was determined between median stream corridor bedrock depth and  
 447 mean summer stream temperature (Figure 59b). ~~However, there, withis~~ strong leverage on the  
 448 linear fit ~~from imparted by~~ the Staunton River datapoint, ~~such that the Spearman rank test was~~  
 449 ~~not significant upon its removal ( $r=-0.42$ ;  $p=0.29$ ).~~



450

451

452 *Figure 9. Mean summer temperature at the downstream monitoring site is shown plotted by a)*  
 453 *elevation, and b) median subwatershed bedrock depth. A significant linear relation was*  
 454 *determined with bedrock depth but not elevation.*

455 **4.4 Baseflow Separation (Index)**

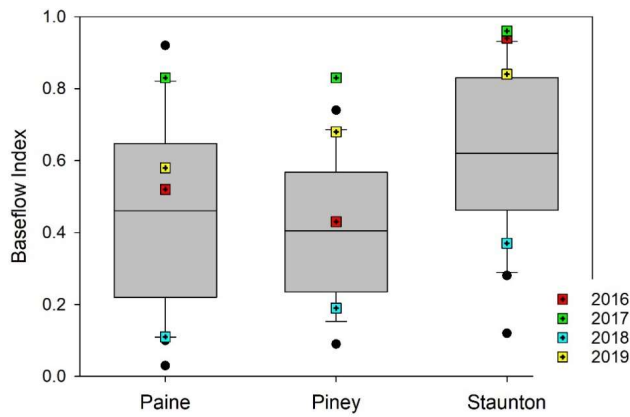
456 The summer season BFI determined for Paine Run, Piney River, and Staunton River over  
 457 the period of flow record show substantial variability, but the median summer BFI ~~over the~~  
 458 period of flow record for Staunton River (0.62) is approximately 50% greater than Paine Run and  
 459 Piney River (0.46 and 0.41, respectively, Table 2). For the primary study years of 2016-2019,  
 460 Staunton River BFI is always largest, and all sites are above their respective interquartile range  
 461 in 2017 but below their interquartile range in 2018 (Figure 10). The anomalously low 2018 BFI  
 462 values can be explained by extremely high summer precipitation that year (Figure S2), resulting  
 463 in total streamflow being dominated by runoff and quickflow as parsed determined by with

464 baseflow separation. Mean summer streamflow over the period of record was highest for Piney  
 465 River and lowest for Pain Run, and overall summer streamflow was most stable for Staunton  
 466 River (lowest coefficient of variation).

467 **Table 2.** The median summer Baseflow Index (BFI), mean summer streamflow, and mean summer  
 468 standard deviation (SD) streamflow for three gaged streams from 1993-2020.

<i>site</i>	<i>median BFI</i>	<i>mean streamflow (L/s)</i>	<i>mean coefficient of streamflow variation</i>
Paine Run	0.46	93.0	1.6
Piney River	0.41	164.4	1.7
Staunton River	0.62	157.3	0.7

469



470

471 *Figure 10. Summer Baseflow Index metrics summarized from 1993-2020 for three streams, with*  
 472 *specific values from the primary study years identified.*

473 **5.0 Discussion**

474 *5.1 Longitudinal Spatial Structure in Observed Bedrock Depth*

475 Seminal groundwater/surface water exchange research has indicated that bedrock  
476 topography along headwater streams may be a first-order control on the arrangement of nested  
477 gaining and losing flowpaths (e.g. Tonina & Buffington, 2009), and increased depth to l(low  
478 permeability) bedrock depth-contacts is recognized as a primary driver of stream disconnection  
479 during dry periods that could be exacerbated by climate change (Ward et al 2020). However,  
480 despite the apparent importance to a range of headwater stream physical processes and cold-  
481 water habitat, local bedrock depth data are almost universally lacking, even in heavily studied  
482 experimental watersheds. Our study provides new inferences regarding the effects of bedrock  
483 depth on stream flow continuity, groundwater exchange and consequent effects on stream  
484 dewatering and temperature patterns at ecologically relevant spatial scales, and temperature  
485 patterns in mountain streams. The combined datasets indicate stream channel bedrock depth  
486 assessments may be necessary to support stream habitat assessments and predictions of stream  
487 connectivity under drought and climate change when existing large-scale geologic datasets are  
488 not of sufficient spatial resolution to support natural resource management applications.

489 Bedrock depth varied substantially within and among several of the eight study SNP  
490 subwatersheds but was predominantly shallow. For half of the subwatersheds (Hughes River,  
491 Meadow Run, ~~Jeremy's~~Jeremys Run, and Hazel River), median bedrock depth along the stream  
492 channel and lateral riparian zone was less than 2 m and did not show notable variability with  
493 distance, outside of one 12.8 m depth to rock location at upper Hazel River (Figure 4). This  
494 anomalous measurement at Hazel was collected lateral to the stream on a valley terrace of  
495 colluvium, in the vicinity of the only cold (approximately 10 °C at land surface) riparian spring

496 that was observed during all HVSR surveys. Bedrock depths of greater than 8 m were found  
497 along the upper Whiteoak Canyon riparian zone as well (Briggs et al 2018a), also associated with  
498 surficial seepage. Two anomalous bedrock depth measurements of 22.9 and 26.8 m were  
499 collected along the Piney River channel, but instead of being associated with groundwater  
500 springs, they coincided with a discrete sections of channel dewatering at baseflow during 2019  
501 and 2021. Therefore, it appears that discrete zones of thick surficial material are the exception  
502 along SNP streams, though they can be important to localized processes such as focused riparian  
503 discharge and streamflow disconnection (latter discussed in Section 5.2).

504         There are several existing sources of bedrock depth data that could potentially be used to  
505 inform headwater stream modeling and habitat assessment, but the accuracy of such datasets  
506 along headwater streams (typically away from existing boreholes) has generally not been  
507 evaluated. We conducted a point-scale comparison of our relatively high-resolution bedrock  
508 depth measurements to the global bedrock depth map of Shangguan et al., (2017) and found that  
509 bedrock depths were almost universally overpredicted at the SNP by large margins (Figure A4).  
510 Specifically, predictions from the global-scale dataset exceeded HVSR measured depths by  
511 +12.2 m (mean), or approximately four times the average bedrock depth (2.9 m). This result may  
512 not be surprising, as Shangguan et al., (2017) recognizes that large scale bedrock depth  
513 interpolations are likely to overpredict shallow bedrock contacts, especially in mountainous  
514 terrain with minimal available borehole data constraints. As-However, given that baseflow  
515 generation is expected to be dominated by shallow groundwater sourced from unconsolidated  
516 sediment in these headwater systems with low permeability bedrock, this differential could our  
517 study highlights that use of large-scale bedrock depth layers may propagate substantial

518 uncertainty into process-based groundwater flow model predictions ~~if the global-scale dataset~~  
519 ~~was used to~~ when used to inform model structure in the absence of local measurements.

520 Publicly available maps of surficial geologic materials are another potential source of  
521 bedrock depth information. High-resolution digital soils maps are now widely available,  
522 including for the catchments of SNP, and these maps do capture some of the general depth to  
523 rock transitions between subwatersheds observed in this study. For example, NRCS (2020)  
524 (<https://websoilsurvey.sc.egov.usda.gov/App/WebSoilSurvey.aspx>, accessed 12/10/2020)  
525 indicate that the Whiteoak Canyon stream corridor is comprised of silts, loams, and stony soils  
526 with a general bedrock depth of approximately 1.2 m., which is in a similar range as most HVSR  
527 measurements made along the upper stream section (Figure 4). However, the generalized soil  
528 units may not offer needed detail regarding site-specific valley sediment thickness for  
529 hydrogeological and ecological studies where information regarding within-watershed variation  
530 is critical. Along lower Piney River, where HVSR data had depths to rock ranging 1.4 to 3.6 m,  
531 the NRCS soils map universally indicates silt and stony material > 2 m. Along Paine Run, where  
532 the stream is often scoured to bedrock, the soils map shows consistent highly permeable sandy  
533 material with > 2 m thickness. This discrepancy is understandable given most of the test pits  
534 were likely substantially further downstream in better terrain for agriculture. In conclusion,  
535 analysis of large-scale patterns from existing soils maps and interpolated/predicted bedrock  
536 depth layers indicates that more precise geophysical mapping of bedrock depth may be needed to  
537 inform stream research and management, particularly in shallow, low-permeability bedrock  
538 terrain.

539 *5.2 Summer Stream Dewatering Related to Bedrock depth*

540 Aligned with the conceptual model of Ward et al., (2018), our central hypothesis was  
541 bedrock depth along the stream corridor acts as a primary control on longitudinal stream  
542 dewatering and flow disconnection during summer low flows (visual example shown in Figure  
543 A3). We postulated that permeable streambed thickness may undulate along mountain stream  
544 channels, and relatively thick sub-stream sediment zones could accommodate the entirety of low  
545 streamflow volumes, locally disconnecting channels during seasonal ~~drydown~~flow recession. We  
546 found mixed support for this simple hypothesis. Hazel River and Hughes River were two of the  
547 three subwatersheds that had dry channel zones just downstream of their respective stream  
548 origination points in 2016, and these two riparian corridors also had their deepest riparian  
549 bedrock depths in those high-elevation areas. However, as discussed above, Whiteoak Canyon  
550 had relatively thick, porous sediment zone near the subwatershed outlet but did not show any  
551 zones of dewatering, nor did lower Staunton River in 2016, 2019, or 2021, despite having the  
552 deepest median bedrock contact. ~~Jeremy's~~Jeremys Run had three mapped dry zones in 2016 (not  
553 surveyed in 2019), yet depth to rock in those areas was only approximately 2 m, though the  
554 HVSR data collection points were not perfectly aligned with the dry patches. To address this  
555 spatial mismatch in stream dewatering and HVSR data, we used the stream dewatering maps to  
556 guide two new high-resolution HVSR surveys in March 2020 along sections of Paine Run and  
557 Piney River with dynamic patterns of channel drying, as described below.

558 When bedrock depth data were collected at high-resolution, even more variability in  
559 bedrock topography/sediment thickness was revealed ~~th~~an in the original larger-scale surveys,  
560 and that finer scale of information was relevant to understanding stream dewatering patterns.  
561 For example, during summer 2019, a 291 m length section of lower Piney River was observed to  
562 be dry, and immediately preceded by 62 m of isolated stream channel pools, and a nearly

563 identical dewatering pattern was observed there in 2021 (Figures [76,87a,c](#)). The upper portion of  
564 this major feature of stream disconnection corresponded directly with a transition in bedrock  
565 depth along the channel from approximately 3 m to adjacent measurements of 27 and 23 m. This  
566 ‘trough’ in the bedrock surface can likely act as a streamwater sink (shown conceptually in  
567 Figure 1b), routing surface water downward to the point of draining the channel locally in the  
568 summers of 2019 and 2021, but not in 2016 when precipitation (groundwater supply) was higher  
569 than normal. Further downstream, the bedrock depth returned to approximately 3 m near the  
570 furthest downstream measurement point, and flowing channel water was again noted during the  
571 drying surveys. Such a section of stream dewatering in the lower watershed would serve to  
572 impede fish passage along Piney River during the lowest flows, likely corresponding to times of  
573 maximum thermal stress when fish mobility is critical to seeking thermal refuge (Magoulick and  
574 Kobza, 2003).

575 Not all variability in bedrock depth below streams associated with stream drying was as  
576 dramatic as the Piney River example but can be important in disconnecting channel habitat in  
577 summer. Paine Run is a more strongly confined stream valley that had 29 discrete zones of  
578 stream channel dewatering during September of 2019 and extensive dewatering in 2021 ([Figures](#)  
579 [65,76,87b,d](#)), when numerous dead brook trout were also noted ([Figures 5,6,7b,d](#)). Paine also  
580 had the greatest total exposed bedrock out of any of the SNP subwatersheds in this study,  
581 indicating a highly constrained valley underflow reservoir. High resolution bedrock depth data  
582 was collected over a Paine Run subreach with seven discrete dry patches ranging from 17 m to  
583 185 m in channel length, with many bordered by zones of isolated pools (Figure [87b](#)). A  
584 comparison of these patterns with bedrock depth along the channel shows the flowing sections of  
585 stream were dominated by exposed bedrock surfaces or thin sediment. However, a notable

586 exception is toward the upstream end of this focus reach, where depth to rock was consistently >  
587 2 m over the run up to a large zone of disconnected channel with some isolated pools (Figure  
588 [87b,d](#)). This result suggests the losses of stream water accumulated over this approximately 80 m  
589 channel distance. In the following downstream contiguous sections of dry channel and/or  
590 isolated pools, bedrock depth averaged a larger 3.3 m, indicating the entirety of streamflow was  
591 accommodated by the subsurface, congruent with our original hypothesis. However, knowledge  
592 of bedrock depth in isolation is clearly not sufficient to predict stream channel gaining, losing,  
593 and disconnection patterns as the stream with the largest average bedrock depth, lower Staunton  
594 River (median depth to rock 3.4 m, Figure 4), was not observed to dewater during any of the  
595 three physical surveys (Figures [65,76](#)).

### 596 *5.3 Summer Stream Temperature and Groundwater Exchange Dynamics*

597 Although headwater stream heat budgets are complex, our data indicates groundwater  
598 connectivity plays an important role when stream temperatures are already close to aquatic  
599 species thermal tolerances. The apparent dominance of shallow (<3 m depth) groundwater  
600 discharge along Whiteoak Canyon contributed to the Briggs et al. (2018b) prediction that the  
601 lower reaches would not provide suitable brook trout habitat by the end of the century given  
602 anticipated atmospheric warming. [Jeremy'sJeremys](#) Run, a long (13.4 km) stream consistently  
603 underlain by a shallow bedrock contact (median depth < 2 m), already shows a 7-d maximum  
604 summer temperature that exceeds expected brook trout tolerances (i.e., >23.3 °C mean weekly  
605 average temperature, Wehrly et al., (2007)) along the lowest reach.

606 The underflow reservoir of headwater stream valleys integrates upgradient and lateral  
607 hillslope groundwater flowpaths, which accumulate with distance when bounded by low  
608 permeability bedrock. The two subwatersheds with largest median bedrock depth along their

609 respective upstream corridors had the coldest mean summer temperatures, with Staunton River  
610 standing out as distinctly colder, and having the only 7-d max temperature below 20 °C (Table  
611 1). There was a significant relation between median bedrock depth and mean summer stream  
612 temperature at the lower stream sites but not with elevation (Figure 5b9), indicating exchange  
613 with groundwater had disrupted the expected elevation control on lower reach cold water habitat.  
614 Surficial hillslope contributing area is often assumed a primary control on potential groundwater  
615 discharge at the stream subreach scale. However, Staunton River also had the second smallest  
616 drainage surface area of all study subwatersheds, and it is often assumed that lateral groundwater  
617 inflow to headwater streams is related to presumed upslope contributing area. Further, Staunton  
618 River did not have an average valley bottom width that was greater than other streams that were  
619 observed to dewater. This apparent conundrum indicates the importance of bedrock depth  
620 (suprabedrock aquifer thickness) in facilitating spatially persistent baseflow generation during  
621 dry times, and we also found that the more narrow headwater stream valleys of this study tended  
622 to have deeper bedrock depth (Figure 5a).

623 Our research indicates that the vertical shallow aquifer dimension, as represented by  
624 bedrock depth, is likely an important control of groundwater storage and connectivity to the  
625 stream corridor. This conclusion is supported by the paired air/water annual temperature signal  
626 metrics, indicating Staunton River sites cluster in the toward stronger, deeper groundwater  
627 influence compared to most observations along the other SNP streams (Figure 98a). Therefore, it  
628 seems there are important tradeoffs between bedrock depth along the stream channel as a driver  
629 of stream dewatering and sediment thickness along the valley floor and hillslopes as a potential  
630 source of stream baseflow.

631 For a more in-depth analysis of the paired bedrock depth and groundwater inflow  
632 controls on headwater summer stream dynamics, Staunton River can be contrasted with Paine  
633 Run. The latter had a similar total drainage surface area to Staunton River with a >5 m (average)  
634 wider stream valley bottom, but a 1.2 m shallower bedrock depth on average. Paine Run had,  
635 showed dozens of dewatered stream channel sections in 2019 and 2021, and had a downstream  
636 boundary summer stream temperature that was 1.4 °C warmer than Staunton River. In addition  
637 to a reduced average bedrock depth, Paine Run had numerous sections of exposed bedrock  
638 adjacent to localized pockets of stream channel alluvium and colluvium (Figure 4, 7), while  
639 extensive colluvial deposits along the Staunton River channel limited exposed bedrock to a few  
640 m-scale sections associated with pool steps (Figure 4). Lower Staunton experienced major debris  
641 flows in June, 1995 (Morgan and Wieczorek, 1996), events that likely created an enhanced local  
642 groundwater reservoir within coarse hillslope material compared to other SNP subwatersheds.

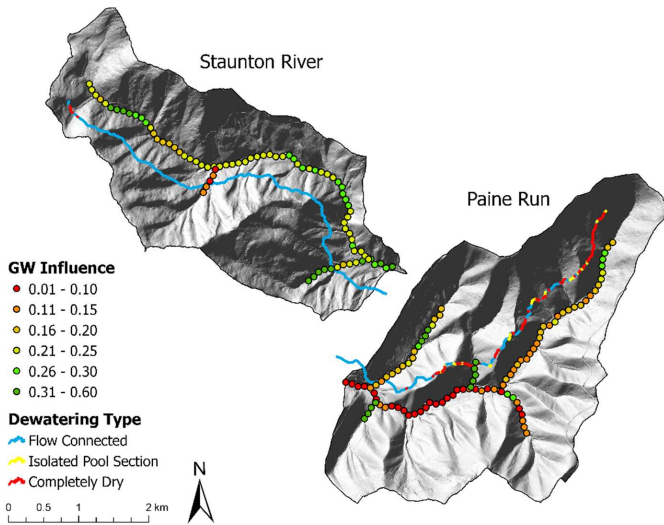
643 Based on the integrated datasets from these two SNP streams, we conclude that  
644 groundwater exchange is a critical factor determining whether headwater streams will warm and  
645 dewater in summer, which in turn is controlled in part by the thickness of supra-bedrock  
646 unconsolidated aquifer. As noted above, annual temperature metrics indicated a consistently  
647 deeper groundwater discharge influence along Staunton River, while Paine Run had annual  
648 signal metrics that mainly indicated reduced and/or more shallow groundwater influence (Figure  
649 9a). Long-term streamflow and baseflow analysis from these streams showed Staunton River  
650 had higher, but more stable summer discharge (Table 1), and substantially higher median  
651 summer BFI (0.62 vs 0.46), indicating greater dominance of groundwater as a generator of  
652 streamflow compared to runoff and quickflow. Previous research in SNP used paired air/stream  
653 water temperature records, precipitation, and landscape characteristics to statistically model

654 'groundwater influence' by year on a scale of 0-1 at the 100-m scale along the streams of this  
655 study, where details are described by Johnson et al., (2017). Although this previous work only  
656 extended to 2015, that year had analogous BFI scores to 2019 for Staunton River (0.88 vs 0.84)  
657 and Paine Run (0.60 vs 0.58). Comparing the 2019 drying survey observations to the 2015 high  
658 spatial resolution modeling of groundwater influence we found that Paine Run was predicted to  
659 have groundwater influenced tributaries, but along the mainstem, where extensive dewatering  
660 was observed, there was substantially reduced modeled groundwater influence compared to the  
661 mainstem of Staunton River (Figure 11). Johnson et al., (2017) also found a negative relation  
662 between valley bottom width and their metrics of groundwater influence on SNP streams. In the  
663 context of our finding that bedrock depth is negatively related to valley bottom width, we find  
664 further support for the hypothesis that thicker headwater stream valley sediments are influential  
665 to baseflow generation in low permeability bedrock settings.

666

667

668



669

670 *Figure 11. The 2019 stream dewatering survey data (lines; this study), plotted offset of the*  
 671 *mainstem, and 100-m groundwater influence predictions (points from Johnson et al., 2017),*  
 672 *plotted along the mainstem and tributaries, of Staunton River and Paine Run.*

673 This observation and model comparison represents another line of evidence that groundwater  
 674 connectivity at the sub-reach scale is key in determining whether local increases in depth to  
 675 bedrock drive channel dewatering at low flow. The impact of reduced underflow groundwater  
 676 supply on stream disconnection is likely exasperated by the extensive zones of exposed bedrock  
 677 along Paine Run (Figure 4, 7d), which locally reduce groundwater mounding in stream valley  
 678 sediments as shown conceptually in Figure 1b, such that abrupt increases in bedrock depth cause  
 679 stream dewatering. Among the eight streams investigated here, Staunton River likely represents  
 680 the most resilient summer cold water habitat, which could not be predicted using bedrock depth  
 681 data alone but necessitated paired assessment of groundwater discharge dynamics.

Formatted: Space After: 12 pt

Formatted: Font: Not Italic

682 **6 Conclusions**

683 In steep mountain valley stream systems underlain by low-permeability bedrock, the  
684 longitudinal underflow reservoir serves as a complex mechanism of streamflow generation,  
685 streamflow losses, and stream temperature control (Figure 1, Supplementary Figure S1). Our  
686 study utilized complimentary geophysical, temperature, and hydrologic data at the scale of eight  
687 subwatersheds to highlight apparent tradeoffs in bedrock depth, shallow groundwater supply, and  
688 the quality of cold-water habitat. Certain mountain stream corridor parameters may be  
689 reasonable to assume or infer from high-resolution topographic data, such as surficial sediment  
690 permeability (based on land surface roughness) and stream valley width, which are primary  
691 controls on whether underflow serves as a net source or sink of stream water (Flinchum et al.,  
692 2018; Ward et al., 2018). However, as shown here, advances in predicting hydrologic  
693 connectivity and thermal variation along mountain stream networks may also require local  
694 evaluation of bedrock depth and stream-groundwater exchange.

695 When local increases in bedrock depth are not balanced by groundwater inflow, streams  
696 may be expected to dewater and disconnect under low flow conditions, and streams with reduced  
697 deeper groundwater influence or shallower-sourced groundwater show warmer summer  
698 temperatures. Contrary to what might be expected, we found that mean summer stream  
699 temperature ~~at~~ was not significantly related to elevation at all lower study boundaries, but instead  
700 was (negatively) related to average stream bedrock depth. Staunton River had the coldest  
701 summer stream temperatures and most pronounced deeper groundwater signatures. However,  
702 that subwatershed was of relatively small total surface area and average valley bottom width.  
703 The defining physical feature of Staunton River was that it had the largest average bedrock depth  
704 of all the eight SNP study streams at 3.4 m, allowing greater overall storage of recharge and

705 baseflow generation. The other two gaged streams had substantially reduced baseflow indices,  
706 indicating streamflow generation was dominated by runoff and quickflow.

707 Overall, SNP streams tended to have consistently shallow bedrock depth, though a subset  
708 were more variable or had spatial trends and discrete features. Observed channel dewatering  
709 patterns during late summer baseflow periods were related to local scale variation in bedrock  
710 depth, such as a discrete feature of greater than 20 m depth observed along Piney River that  
711 caused repeated streamflow disconnection. However, in other streams more subtle bedrock depth  
712 variation also caused channel dewatering, indicating the importance of local hydrogeological  
713 context in determining the importance of bedrock depth on streamflow connectivity. For  
714 example, patchy 2-4 m deposits of sediment adjacent to exposed bedrock along Paine Run  
715 caused extensive summer dewatering in 2019 and 2021, and during the latter survey many dead  
716 brook trout were noted in the disconnected sections. Paine and Piney also showed enhanced  
717 dewatering during the summers of 2019 and 2021 compared to the wetter 2016 summer,  
718 demonstrating the additional control of recent precipitation on stream disconnection in headwater  
719 systems that do not efficiently store water.

720 Lateral groundwater inflow through high permeability, unconsolidated sediments is a  
721 critical component of headwater stream baseflow (Tran et al., 2020). Shallow, low permeability  
722 bedrock can constrain lateral flowpaths and underflow to the near surface critical zone, where it  
723 is highly sensitive to enhanced evapotranspiration, temperature increase, and drought under  
724 climate change (Condon et al., 2020; Hare et al., 2021). As it becomes increasingly important to  
725 understand and predict the resilience of mountain cold-water stream habitat at a fine spatial  
726 grain, continued coupled advances in geophysical characterization, stream temperature  
727 monitoring, and groundwater exchange analysis are needed.

728 **Data Availability**

729 The data described in this manuscript are available at: [doi.org/10.5066/F7B56H72](https://doi.org/10.5066/F7B56H72),  
730 [doi.org/10.5066/F7JW8C04](https://doi.org/10.5066/F7JW8C04), and [doi.org/10.5066/P9IJMGIB](https://doi.org/10.5066/P9IJMGIB)

731 **Author contribution**

732 *Conceptualization*: M.A. Briggs, Z.C. Johnson, C.D. Snyder, N.P. Hitt; *Investigation*: M.A.  
733 Briggs, P. Goodling, Z.C. Johnson, C.D. Snyder, K.M. Rogers, N.P. Hitt; *Visualization*: M.A.  
734 Briggs, K.M. Rogers, P. Goodling, J.B. Fair, C.D. Snyder. All authors contributed to the formal  
735 analysis and varied stages of writing.

736 **Competing interests**

737 The authors declare that they have no conflict of interest.

738 **Acknowledgments**

739 The authors gratefully acknowledge support from Natural Resource Preservation Program and  
740 the U.S. Geological Survey (USGS) Chesapeake Bay Priority Ecosystems Science and Fisheries  
741 Program. We also thank the Shenandoah National Park Staff for site access and general support  
742 and field support from John Lane, David Nelms, Adam Haynes, Erin Snook, David Weller, Evan  
743 Rodway, Jacob Roach, Matt Marshall, Joe Dehnert, and Mary Mandt. Any use of trade, firm, or  
744 product names is for descriptive purposes only and does not imply endorsement by the U.S.  
745 Government.

746

747 **References**

- 748 Barlow, P.M., Cunningham, W.L., Zhai, T., Gray, M., 2014. U.S. Geological Survey  
749 Groundwater Toolbox, a graphical and mapping interface for analysis of hydrologic data  
750 (version 1.0): User guide for estimation of base flow, runoff, and groundwater recharge  
751 from streamflow data: U.S. Geological Survey Techniques a. B. 3 B10, 27.  
752 <https://doi.org/http://dx.doi.org/10.3133/tm3B10>
- 753 Briggs, M.A., Johnson, Z.C., Snyder, C.D., Hitt, N.P., Kurylyk, B.L., Lautz, L., Irvine, D.J.,  
754 Hurley, S.T., Lane, J.W., 2018a. Inferring watershed hydraulics and cold-water habitat  
755 persistence using multi-year air and stream temperature signals. *Sci. Total Environ.* 636.  
756 <https://doi.org/10.1016/j.scitotenv.2018.04.344>
- 757 Briggs, M.A., Lane, J.W., Snyder, C.D., White, E.A., Johnson, Z.C., Nelms, D.L., Hitt, N.P.,  
758 2018b. Shallow bedrock limits groundwater seepage-based headwater climate refugia.  
759 *Limnologia* 68, 142–156. <https://doi.org/10.1016/j.limno.2017.02.005>
- 760 Briggs, M.A., Lane, J.W., Snyder, C.D., White, E.A., Johnson, Z.C., Nelms, D.L., Hitt, N.P.,  
761 2017. Seismic data for study of shallow mountain bedrock limits seepage-based headwater  
762 climate refugia, Shenandoah National Park, Virginia: U.S. Geological Survey data release.  
763 <https://doi.org/10.5066/F7JW8C04>
- 764 Bundschuh, J., 1993. Modeling annual variations of spring and groundwater temperatures  
765 associated with shallow aquifer systems Computer model. *J. Hydraul. Eng.* 142, 427–444.
- 766 Burns, D.A., Murdoch, P.S., Lawrence, G.B., Michel, R.L., 1998. Effect of groundwater springs  
767 on NO<sub>3</sub><sup>-</sup> concentrations during summer in Catskill Mountain streams. *Water Resour. Res.*  
768 34, 1987–1996. [https://doi.org/Cited By \(since 1996\) 98Export Date 4 April 2012](https://doi.org/Cited%20By%20(since%201996)%2098Export%20Date%204%20April%202012)
- 769 Condon, L.E., Atchley, A.L., Maxwell, R.M., 2020. Evapotranspiration depletes groundwater  
770 under warming over the contiguous United States. *Nat. Commun.* 11.  
771 <https://doi.org/10.1038/s41467-020-14688-0>
- 772 Costigan, K.H., Jaeger, K.L., Goss, C.W., Fritz, K.M., Goebel, P.C., 2016. Understanding  
773 controls on flow permanence in intermittent rivers to aid ecological research: integrating  
774 meteorology, geology and land cover. *Ecohydrology* 9, 1141–1153.  
775 <https://doi.org/10.1002/eco.1712>
- 776 Covino, T., 2017. Hydrologic connectivity as a framework for understanding biogeochemical  
777 flux through watersheds and along fluvial networks. *Geomorphology* 277, 133–144.  
778 <https://doi.org/10.1016/j.geomorph.2016.09.030>
- 779 DeKay, R.H., 1972. Development of ground-water supplies in Shenandoah National Park,  
780 Virginia. *Virginia Div. Miner. Resour. Rep.* 10, 158.
- 781 Edge, C.B., Fortin, M.J., Jackson, D.A., Lawrie, D., Stanfield, L., Shrestha, N., 2017. Habitat  
782 alteration and habitat fragmentation differentially affect beta diversity of stream fish  
783 communities. *Landsc. Ecol.* 32, 647–662. <https://doi.org/10.1007/s10980-016-0472-9>
- 784 Fausch, K.D., Torgersen, C.E., Baxter, C. V., Li, H.W., 2002. Landscapes to riverscapes:  
785 Bridging the gap between research and conservation of stream fishes. *Bioscience* 52, 483–  
786 498. [https://doi.org/10.1641/0006-3568\(2002\)052\[0483:LTRBTG\]2.0.CO;2](https://doi.org/10.1641/0006-3568(2002)052[0483:LTRBTG]2.0.CO;2)

787 Flinchum, B.A., Holbrook, W.S., Grana, D., Parsekian, A.D., Carr, B.J., Hayes, J.L., Jiao, J.,  
788 2018. Estimating the water holding capacity of the critical zone using near-surface  
789 geophysics. *Hydrol. Process.* 32, 3308–3326. <https://doi.org/10.1002/hyp.13260>

790 Furze, S., Sullivan, A.M.O., Allard, S., Pronk, T., Curry, R.A., 2021. A High-Resolution ,  
791 Random Forest Approach to Mapping Depth-to-Bedrock across Shallow Overburden and  
792 Post-Glacial Terrain. *Remote Sens.* 13, 1–23. <https://doi.org/10.3390/rs13214210>

793 Goodling, P.J., Briggs, M.A., White, E.A., Johnson, Z.C., Haynes, A.B., Nelms, D.L., Lane,  
794 J.W., 2020. Passive seismic data collected along headwater stream corridors in Shenandoah  
795 National Park in 2016 - 2020: US Geol. Surv. Data Release.  
796 <https://doi.org/doi.org/10.5066/P9IJMGIB>

797 Hare, D.K., Helton, A.M., Johnson, Z.C., Lane, J.W., Briggs, M.A., 2021. Continental-scale  
798 analysis of shallow and deep groundwater contributions to streams. *Nat. Commun.* 1–10.  
799 <https://doi.org/10.1038/s41467-021-21651-0>

800 Herzog, S.P., Ward, A.S., Wondzell, S.M., 2019. Multiscale Feature-feature Interactions Control  
801 Patterns of Hyporheic Exchange in a Simulated Headwater Mountain Stream. *Water*  
802 *Resour. Res.* 55, 10976–10992. <https://doi.org/10.1029/2019WR025763>

803 Hopper, G.W., Gido, K.B., Pennock, C.A., Hedden, S.C., Frenette, B.D., Barts, N., Hedden,  
804 C.K., Bruckerhoff, L.A., 2020. Nowhere to swim: interspecific responses of prairie stream  
805 fishes in isolated pools during severe drought. *Aquat. Sci.* 82, 1–15.  
806 <https://doi.org/10.1007/s00027-020-0716-2>

807 Ilja Van Meerveld, H.J., Kirchner, J.W., Vis, M.J.P., Assendelft, R.S., Seibert, J., 2019.  
808 Expansion and contraction of the flowing stream network alter hillslope flowpath lengths  
809 and the shape of the travel time distribution. *Hydrol. Earth Syst. Sci.* 23, 4825–4834.  
810 <https://doi.org/10.5194/hess-23-4825-2019>

811 Jencso, K.G., McGlynn, B.L., Gooseff, M.N., Bencala, K.E., Wondzell, S.M., 2010. Hillslope  
812 hydrologic connectivity controls riparian groundwater turnover: Implications of catchment  
813 structure for riparian buffering and stream water sources. *Water Resour. Res.* 46, 1–18.  
814 <https://doi.org/10.1029/2009WR008818>

815 Johnson, Z.C., Johnson, B.G., Briggs, M.A., Devine, W.D., Snyder, C.D., Hitt, N.P., Hare, D.K.,  
816 Minkova, T. V., 2020. Paired air-water annual temperature patterns reveal hydrogeological  
817 controls on stream thermal regimes at watershed to continental scales. *J. Hydrol.* 587,  
818 124929. <https://doi.org/10.1016/j.jhydrol.2020.124929>

819 Johnson, Z.C., Snyder, C.D., Hitt, N.P., 2017. Landformfeatures and seasonal precipitation  
820 predict shallow groundwater influence on temperature in headwater streams. *Water Resour.*  
821 *Res.* 53, 5788–5812. <https://doi.org/10.1002/2017WR020455>

822 Kauffman, L.J., Yager, R.M., Reddy, J.E., 2018. Sediment and Aquifer Characteristics of  
823 Quaternary Sediments in the Glaciated Conterminous United States: U.S. Geol. Surv. data  
824 release. <https://doi.org/10.5066/F7HH6J8X>

825 Labbe, T.R., Fausch, K.D., 2000. Dynamics of intermittent stream habitat regulate persistence of  
826 a threatened fish at multiple scales. *Ecol. Appl.* 10, 1774–1791.  
827 <https://doi.org/10.1890/1051-0761>

- 828 Lapham, W.W., 1989. Use of temperature profiles beneath streams to determine rates of vertical  
829 ground-water flow and vertical hydraulic conductivity. *US Geol. Surv. Water-Supply Pap.*  
830 2337.
- 831 Larkin, R.G., Sharp, J.M., 1992. On the relationship between river-basin geomorphology, aquifer  
832 hydraulics, and ground-water flow direction in alluvial aquifers. *Geol. Soc. Am. Bull.* 104,  
833 1608–1620.
- 834 Litwin, D.G., Tucker, G.E., Barnhart, K.R., Harman, C.J., 2022. Groundwater Affects the  
835 Geomorphic and Hydrologic Properties of Coevolved Landscapes. *J. Geophys. Res. Earth*  
836 *Surf.* 127, 1–36. <https://doi.org/10.1029/2021JF006239>
- 837 Lynch, D.D., 1987. Hydrologic conditions and trends in Shenandoah National Park, Virginia,  
838 1983–84. *Water- Resour. Investig. Rep.* 87–4131.
- 839 Magoulick, D.D., Kobza, R.M., 2003. The role of refugia for fishes during drought: A review  
840 and synthesis. *Freshw. Biol.* 48, 1186–1198. [https://doi.org/10.1046/j.1365-](https://doi.org/10.1046/j.1365-2427.2003.01089.x)  
841 [2427.2003.01089.x](https://doi.org/10.1046/j.1365-2427.2003.01089.x)
- 842 McLachlan, P.J., Chambers, J.E., Uhlemann, S.S., Binley, A., 2017. Geophysical  
843 characterisation of the groundwater–surface water interface. *Adv. Water Resour.* 109, 302–  
844 319. <https://doi.org/10.1016/j.advwatres.2017.09.016>
- 845 Meisner, J.D., Rosenfeld, J.S., Regier, H.A., 1988. The Role of Groundwater in the Impact of  
846 Climate Warming on Stream Salmonines. *Fisheries* 13, 2–8.
- 847 Nelms, D.L., Moberg, R.M., 2010. Preliminary Assessment of the Hydrogeology and  
848 Groundwater Availability in the Metamorphic and Siliciclastic Fractured-Rock Aquifer  
849 Systems of Warren County, Virginia. *U.S. Geol. Surv. Investig. Rep.* 2010–5190.
- 850 O’Sullivan, A.M., Devito, K.J., Ogilvie, J., Linnansaari, T., Pronk, T., Allard, S., Curry, R.A.,  
851 2020. Effects of Topographic Resolution and Geologic Setting on Spatial Statistical River  
852 Temperature Models. *Water Resour. Res.* 56, 1–23. <https://doi.org/10.1029/2020WR028122>
- 853 Odom, W.E., Doctor, D.H., Burke, C.E., Cox, C.L., 2021. Using high-resolution LiDAR and  
854 deep learning models to generate minimum thickness maps of surficial sediments, in:  
855 *Geological Society of America Abstracts with Programs*, v. 53. Portland, OR.  
856 <https://doi.org/10.1130/abs/2021AM-367681>
- 857 Payn, R.A., Gooseff, M.N., McGlynn, B.L., Bencala, K.E., Wondzell, S.M., 2009. Channel  
858 water balance and exchange with subsurface flow along a mountain headwater stream in  
859 Montana, United States. *Water Resour. Res.* 45. <https://doi.org/10.1029/2008wr007644>
- 861 Pelletier, J.D., Broxton, P.D., Hazenberg, P., Zeng, X., Troch, P.A., Niu, G.-Y., Williams, Z.,  
862 Brunke, M.A., Gochis, D., 2016. A gridded global data set of soil, intact regolith, and  
863 sedimentary deposit thicknesses for regional and global land surface modeling. *J. Adv.*  
864 *Model. Earth Syst.* 8. <https://doi.org/10.1002/2015MS000526>
- 865 Plummer, L.N., Busenberg, E., Bohlke, J.K., Nelms, D.L., Michel, R.L., Schlosser, P., 2001.  
866 Groundwater residence times in Shenandoah National Park, Blue Ridge Mountains,  
867 Virginia, USA: a multi-tracer approach. *Chem. Geol.* 179, 93–111.

868 Rolls, R.J., Leigh, C., Sheldon, F., 2012. Mechanistic effects of low-flow hydrology on riverine  
869 ecosystems: Ecological principles and consequences of alteration. *Freshw. Sci.* 31, 1163–  
870 1186. <https://doi.org/10.1899/12-002.1>

871 Shangguan, W., Hengl, T., Mendes de Jesus, J., Yuan, H., Dai, Y., 2017. Mapping the global  
872 depth to bedrock for land surface modeling. *J. Adv. Model. Earth Syst.* 9, 65–88.  
873 <https://doi.org/10.1002/2016MS000686>

874 Sidle, R.C., Tsuboyama, Y., Noguchi, S., Hosoda, I., Fujieda, M., Shimizu, T., 2000. Stormflow  
875 generation in steep forested headwaters: A linked hydrogeomorphic paradigm. *Hydrol.*  
876 *Process.* 14, 369–385. [https://doi.org/10.1002/\(SICI\)1099-1085\(20000228\)14:3<369::AID-  
877 HYP943>3.0.CO;2-P](https://doi.org/10.1002/(SICI)1099-1085(20000228)14:3<369::AID-HYP943>3.0.CO;2-P)

878 Singha, K., Navarre-Sitchler, A., 2021. The importance of groundwater in critical zone science.  
879 *Groundwater* 1–8. <https://doi.org/10.1111/gwat.13143>

880 Snyder, C.D., Hitt, N.P., Johnson, Z.C., 2017. Air-water temperature data for the study of  
881 groundwater influence on stream thermal regimes in Shenandoah National Park, Virginia:  
882 U.S. Geological Survey data release. <https://doi.org/https://doi.org/10.5066/F7B56H72>

883 Snyder, C.D., Hitt, N.P., Young, J.A., 2015. Accounting for groundwater in stream fish thermal  
884 habitat responses to climate change. *Ecol. Appl.* 00, 281–304.

885 Snyder, C.D., Webb, J.R., Young, J.A., Johnson, Z.B., Jewell, S., Survey, U.S.G., 2013.  
886 Significance of Headwater Streams and Perennial Springs in Ecological Monitoring in  
887 Shenandoah National Park. Open-File Rep. 2013–1178 46.

888 Southworth, S., Aleinikoff, J.N., Bailey, C.M., Burton, W.C., Crider, E.A., Hackley, P.C.,  
889 Smoot, J.P., Tollo, R.P., 2009. Geologic Map of the Shenandoah National Park Region,  
890 Virginia. US Geol. Surv. Open-File Rep. 2009–1153 1.

891 Stonestrom, D.A., Constantz, J., 2003. Heat as a Tool for Studying the Movement of Ground  
892 Water Near Streams. *U.S. Geol. Surv. Circ.*, 1260, 1–6. 96.

893 Sullivan, C., Vokoun, J., Helton, A., Briggs, M.A., Kurylyk, B., 2021. An ecohydrological  
894 typology for thermal refuges in streams and rivers. *Ecohydrology*.  
895 <https://doi.org/10.1002/eco.2295>

896 Tiwari, T., Buffam, I., Sponseller, R.A., Laudon, H., 2017. Inferring scale-dependent processes  
897 influencing stream water biogeochemistry from headwater to sea. *Limnol. Oceanogr.* 62,  
898 S58–S70. <https://doi.org/10.1002/lno.10738>

899 Tonina, D., Buffington, J.M., 2009. Hyporheic Exchange in Mountain Rivers I: Mechanics and  
900 Environmental Effects. *Geogr. Compass* 3, 1063–1086. [https://doi.org/10.1111/j.1749-  
901 8198.2009.00226.x](https://doi.org/10.1111/j.1749-8198.2009.00226.x)

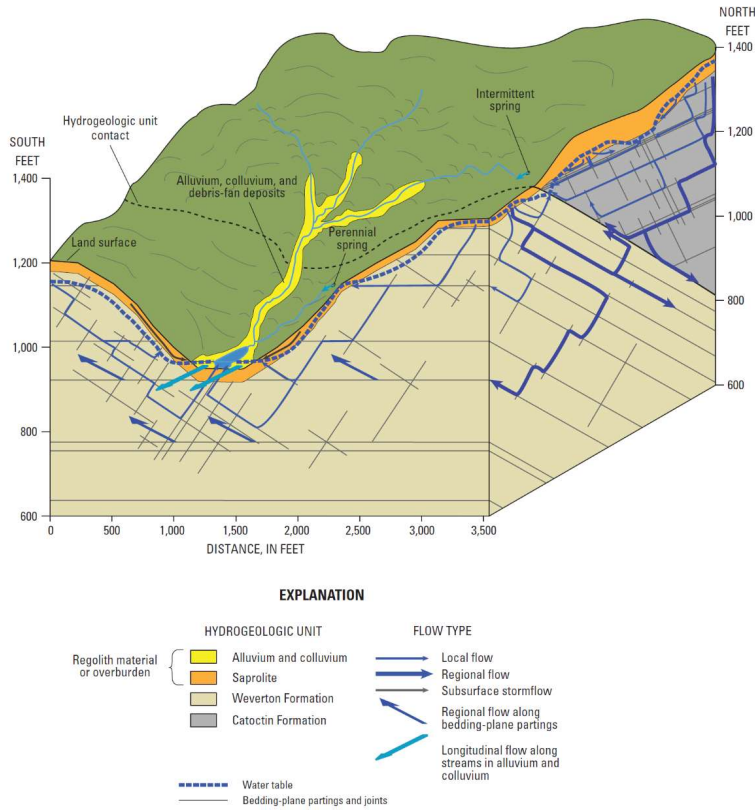
902 Tran, H., Zhang, J., Cohard, J.M., Condon, L.E., Maxwell, R.M., 2020. Simulating  
903 Groundwater-Streamflow Connections in the Upper Colorado River Basin. *Groundwater*  
904 58, 392–405. <https://doi.org/10.1111/gwat.13000>

905 Ward, A.S., Schmadel, N.M., Wondzell, S.M., 2018. Simulation of dynamic expansion,  
906 contraction, and connectivity in a mountain stream network. *Adv. Water Resour.* 114, 64–  
907 82. <https://doi.org/10.1016/j.advwatres.2018.01.018>

- 908 Ward, A.S., Wondzell, S.M., Schmadel, N.M., Herzog, S.P., 2020. Climate Change Causes River  
909 Network Contraction and Disconnection in the H.J. Andrews Experimental Forest, Oregon,  
910 USA. *Front. Water* 2, 1–10. <https://doi.org/10.3389/frwa.2020.00007>
- 911 Warix, S.R., Godsey, S.E., Lohse, K.A., Hale, R.L., 2021. Influence of groundwater and  
912 topography on stream drying in semi-arid headwater streams. *Hydrol. Process.* 35, 1–18.  
913 <https://doi.org/10.1002/hyp.14185>
- 914 Weekes, A.A., Torgersen, C.E., Montgomery, D.R., Woodward, A., Bolton, S.M., 2015.  
915 Hydrologic response to valley-scale structure in alpine headwaters. *Hydrol. Process.* 29,  
916 356–372. <https://doi.org/10.1002/hyp.10141>
- 917 Wehrly, K., Wang, L., Mitro, M., 2007. Field-based estimates of thermal tolerance limits for  
918 trout: incorporating exposure time and temperature fluctuation. *Trans. Am. Fish. Soc.* 136,  
919 365–374.
- 920 Winter, T.C., Harvey, J.W., Franke, O.L., Alley, W.M., 1998. Ground water and surface water: a  
921 single resource. *U. S. Geol. Surv. Circ.* 1139 79.
- 922 Wohl, E., 2017. Connectivity in rivers. *Prog. Phys. Geogr.* 41, 345–362.  
923 <https://doi.org/10.1177/0309133317714972>
- 924 Wu, L., Gomez-Velez, J.D., Krause, S., Singh, T., Wörman, A., Lewandowski, J., 2020. Impact  
925 of Flow Alteration and Temperature Variability on Hyporheic Exchange. *Water Resour.*  
926 *Res.* 56. <https://doi.org/10.1029/2019WR026225>
- 927 Yanamaka, H., Takemura, M., Ishida, H., Niwa, M., 1994. Characteristics of long-period  
928 microtremors and their applicability in exploration of deep sedimentary layers. *Bull. Seism.*  
929 *Soc. Am.* 84, 1831–1841.
- 930 Zimmer, M.A., McGlynn, B.L., 2017. Bidirectional stream–groundwater flow in response to  
931 ephemeral and intermittent streamflow and groundwater seasonality. *Hydrol. Process.* 31,  
932 3871–3880. <https://doi.org/10.1002/hyp.11301>

933

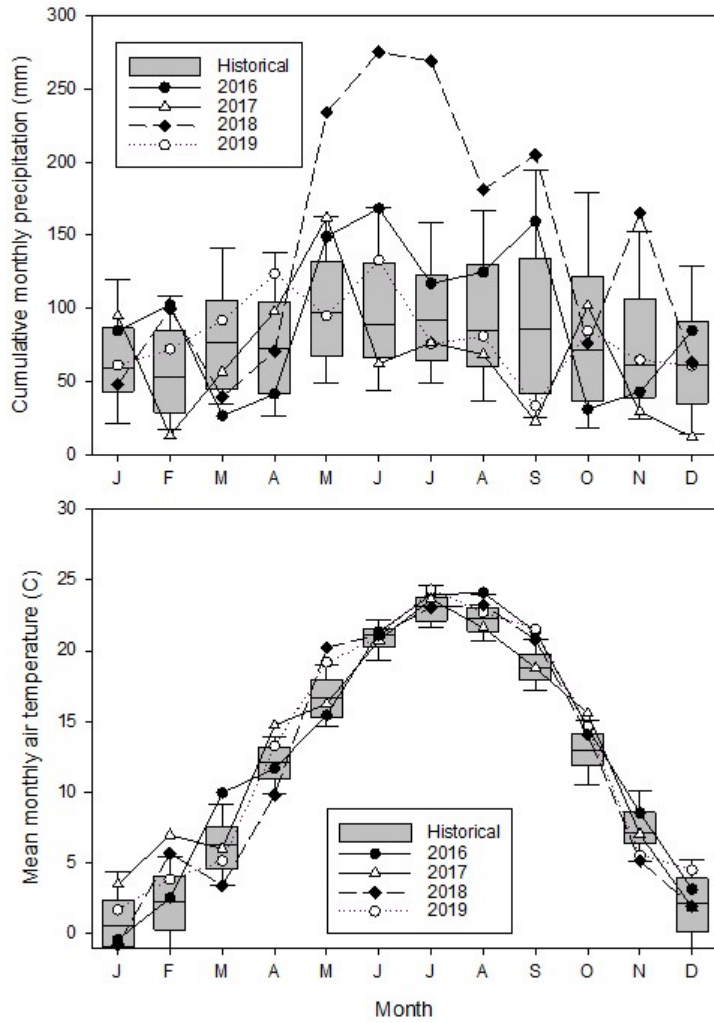
934 **Appendix A**



935

936 Figure A1. The headwater streams of Shenandoah National Park, Virginia, USA are expected to  
937 flow over coarse alluvium and colluvium and have connectivity to shallow hillslope groundwater  
938 and underflow, but reduced connectivity to deeper bedrock groundwater (Modified Figure 26 in  
939 (Nelms and Moberg, 2010) *U.S. Geol. Surv. Investigations Rep.* 2010–5190.

940



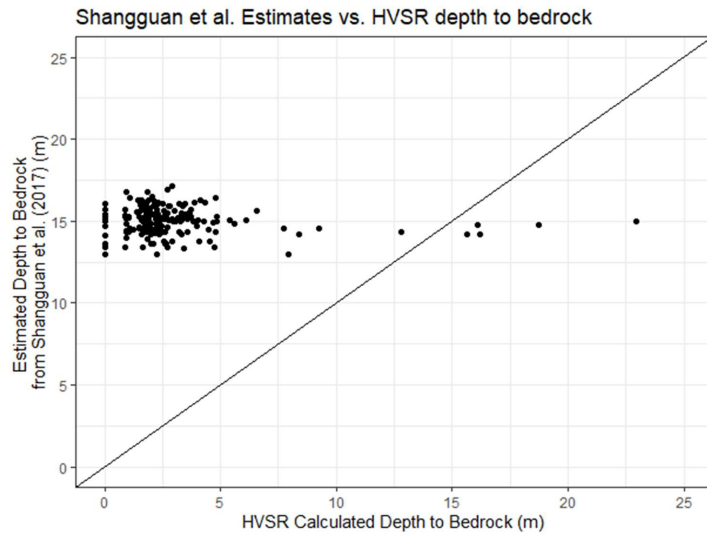
941  
 942 Figure A2. Monthly precipitation and air temperature data derived from the Luray weather  
 943 station (GHCND:USC00445096) located within Shenandoah National Park. Box plots show the  
 944 distribution of values for the period of record (1942-2020) with the limits of the box containing  
 945 50% of the values, whiskers containing 90% of the values, and solid line in boxes depicting the  
 946 median value. The lines represent values for the four primary study years.

947



948

949 Figure A3. Images from the same vantage point along Paine Run during a) high and b) low flow  
950 times, the latter showing channel dewatering associated with a deposit of coarse alluvium across  
951 the channel.



952  
 953 Figure A4: Comparison between bedrock depth modeled for the globe by Shangguan et al.,  
 954 (2017) at a 250m resolution and the HVSr-calculated depths to bedrock in this study.  
 955

956 **Appendix B**

957 Table B1. Summer stream temperature metrics for each study subwatershed determined from the  
 958 data set of Snyder et al. (2017), doi.org/10.5066/F7B56H72.

Subwatershed	SiteID	Easting	Northing	Downstream Distance (m)	summer mean (°C)	7-d min (°C)	7-d max (°C)	Stdev (°C)
Hughes	HUR1MP	730038	4276000	242.50	13.43	11.50	16.07	0.98
Hughes	HUR3LCP	731058	4275970	1634.44	15.73	13.23	18.21	1.24
Hughes	HUR5LCP	732278	4275850	3308.93	16.21	13.48	18.62	1.24
Hughes	HUR6MP	733348	4275060	5163.46	16.39	13.86	17.95	1.13
Hughes	HUR12MP	733698	4274880	5620.73	16.79	14.09	18.34	1.24
Hughes	HUR8LCP	733988	4274619	6219.50	18.80	15.19	21.49	1.57
Hughes	HUR9LCP	733968	4274529	6284.35	17.59	14.49	20.09	1.34
Hughes	HUR10MP	734928	4273520	8187.04	18.05	15.01	20.05	1.40
Hughes	HUR13MP	735258	4273330	8667.16	18.68	15.15	21.18	1.62
Hazel	HZR1MP	735158	4278560	707.45	16.80	13.26	19.75	1.46
Hazel	HZR3LCP	735498	4278760	1190.18	16.74	13.08	19.41	1.50
Hazel	HZR11MP	736378	4279640	2951.89	18.16	15.34	20.32	1.52

Hazel	HZR5MP	736638	4279790	3331.66	17.59	13.59	20.62	1.67
Hazel	HZR6MP	737498	4279059	5095.01	18.16	14.03	21.40	1.74
Hazel	HZR7MP	738048	4277990	6820.13	18.48	14.50	21.77	1.72
Hazel	HZR9MP	738368	4277620	7478.33	18.50	14.74	21.72	1.63
Jeremy'sJeremys	JR1MP	734618	4293430	102.97	15.48	12.42	18.74	1.41
Jeremy'sJeremys	JR2MP	733908	4293130	1268.08	16.49	13.38	19.42	1.38
Jeremy'sJeremys	JR4MP	732498	4292250	3699.53	16.84	14.23	18.22	1.11
Jeremy'sJeremys	JR5MP	731778	4290670	5961.22	17.54	14.15	20.24	1.43
Jeremy'sJeremys	JR13MP	731498	4289490	7506.87	18.16	14.57	21.28	1.67
Jeremy'sJeremys	JR7MP	730068	4288080	10327.83	18.76	16.79	21.07	1.10
Jeremy'sJeremys	JR9LCP	729888	4288080	10539.49	17.78	15.33	20.01	1.04
Jeremy'sJeremys	JR12MP	728758	4288080	12030.09	18.61	14.46	22.08	1.73
Jeremy'sJeremys	JR10MP	727758	4288440	13376.47	19.55	14.93	23.55	1.98
Meadow	MR0MP	695318	4228150	0.00	14.16	12.01	15.57	1.07
Meadow	MR1MP	695038	4227980	217.46	16.82	13.82	18.39	1.28
Meadow	MR2MP	694678	4227520	979.43	17.11	13.71	18.78	1.48
Meadow	MR9MP	693488	4227270	2757.87	18.10	15.34	19.71	1.31
Meadow	MR4LCP	693428	4227240	2854.69	17.01	13.92	19.02	1.44
Meadow	MR8MP	693078	4226450	4036.50	17.53	14.32	19.48	1.35
Meadow	MR6LCP	692918	4226170	4446.20	17.08	14.34	19.32	1.29
Meadow	MR7MP	691738	4225700	6209.68	18.37	15.33	20.44	1.44
Paine	PAR1MP	696938	4232031	249.71	16.86	13.96	18.72	1.36
Paine	PARB1	696718	4231390	1115.08	17.20	14.81	18.70	1.15
Paine	PAR2MP	696468	4231210	1542.16	17.15	15.22	18.61	1.03
Paine	PAR3MP	695685	4230400	3169.18	17.48	14.93	19.28	1.15
Paine	PAR5LCP	695369	4230040	3861.10	17.87	15.01	19.53	1.32
Paine	PAR9MP	694568	4229850	5016.00	18.04	15.43	19.60	1.12
Paine	PAR6MP	694218	4229700	5563.29	18.39	14.86	20.32	1.52
Paine	PAR10MP	694068	4229730	5829.23	18.62	14.71	20.50	1.65
Paine	PARB2	693248	4230140	7055.48	18.60	14.54	20.57	1.67
Paine	PAR8MP	693137	4230180	7122.47	18.84	14.50	20.91	1.97
Piney	PIR1MP	736308	4292604	402.61	15.67	12.24	19.16	1.65
Piney	PIR3LCP	736218	4291980	1199.93	16.43	12.76	19.78	1.65
Piney	PIR4MP	735598	4291160	2480.47	16.55	13.24	19.65	1.51
Piney	PIR5MP	735458	4290050	3955.00	16.82	13.62	19.97	1.48
Piney	PIR6MP	736408	4289180	5862.79	17.74	15.87	20.49	1.15
Piney	PIR7MP	736748	4288300	7115.97	17.40	15.07	20.22	1.17
Piney	PIR8MP	737538	4287390	8756.79	17.88	14.63	20.55	1.39
Staunton	SR1MP	725248	4260810	477.07	14.64	11.96	17.33	1.32
Staunton	SR2MP	725908	4260450	1412.13	15.16	12.34	18.15	1.44
Staunton	SR5MP	726948	4259890	2907.57	15.92	13.03	19.08	1.51

Staunton	SR6MP	728018	4259921	4398.87	16.45	13.48	19.38	1.48
Staunton	SR10MP	728598	4259660	5220.08	17.12	13.88	19.84	1.48
Staunton	SR7MP	728718	4259390	5627.21	17.09	13.99	20.02	1.52
Staunton	SR9MP	729448	4258420	7519.72	17.41	14.57	19.88	1.33
White Oak	WOC1MP	728788	4273701	469.03	13.51	11.85	14.91	0.74
White Oak	WOC3MP	728998	4273160	1237.37	15.43	12.67	17.90	1.29
White Oak	WOC4MP	729268	4272400	2307.96	15.71	12.52	18.58	1.48
White Oak	WOC5MP	730288	4271180	4428.05	17.90	14.23	21.16	1.77
White Oak	WOC7LCP	730758	4270690	5302.94	18.69	15.02	22.07	1.79
White Oak	WOC8MP	730948	4269150	7356.87	18.29	15.88	19.78	1.07
White Oak	WOCB	731018	4269110	7448.09	18.71	16.04	21.18	1.28

959  
960  
961  
962  
963  
964  
965  
966  
967  
968  
969